NASA TECHNICAL MEMORANDUM

NASA TM X-71618

NASA TM X-71618

INTERIM PREDICTION METHOD FOR JET NOISE

by James R. Stone
Lewis Research Center
Cleveland, Ohio 44135

INTERIM PREDICTION METHOD FOR JET NOISE

by James R. Stone

Lewis Research Center

ABSTRACT

This report provides a method of predicting jet noise for a wide range of nozzle geometries and operating conditions of interest for aircraft engines. A limited review of jet noise theory, data and existing prediction methods has been made, and based on this information a new interim method of jet noise prediction is proposed. This report identifies problem areas where further research is needed to improve the prediction method. This method predicts only the noise generated by the exhaust jets mixing with the surrounding air and does not include other noises emanating from the engine exhaust, such as combustion and machinery noise generated inside the engine (i.e., core noise). It does, however, include thrust reverser noise. Prediction relations are provided for conical nozzles, plug nozzles, coaxial nozzles and slot nozzles. For completeness, until further investigations are performed, previously published relations are proposed herein for multi-tube and multi-lobed suppressor nozzles with and without ejectors. For most of these configurations, the effects of nozzle size, jet velocity, jet temperature, and forward (flight) velocity are included in the predictions.

INTERIM PREDICTION METHOD FOR JET NOISE

by James R. Stone

Lewis Research Center

E-8112

SUMMARY

This report provides a method of predicting jet noise for a wide range of nozzle geometries and operating conditions of interest for aircraft engines. This prediction procedure is developed in support of the NASA Aircraft Noise Prediction Program. The prediction method deals only with the noise generated by the exhaust jets mixing with the surrounding air and does not include other noises emanating from the engine exhaust, such as combustion and machinery noise generated inside the engine (i.e., core noise); it does, however, include thrust reverser noise.

Jet noise theory, data, and existing prediction methods were reviewed; however, this review was not exhaustive due to time constraints. Based on this information a new interim method of jet noise prediction is proposed. This report identifies problem areas where further research is needed to improve the prediction method. Experimental data over a wide range of test conditions are shown to verify the prediction method. Jet noise predictions are given for conical nozzles, plug nozzles, coaxial nozzles, slot nozzles and thrust reversers. For completeness, until further investigations are performed, previously published relations are proposed herein for multi-tube and multi-lobe suppressor nozzles with and without ejectors. For most of the configurations, the effects of nozzle size, jet velocity, jet temperature, and vehicle forward speed are included in the predictions.

INTRODUCTION

Accurate noise prediction methods are now required in order to predict the environmental impact of airport operations on the surrounding communities, and for realistic design of new aircraft as well as development of noise reduction modifications for existing aircraft. A prediction method is presented in response to the need for predicting jet noise as a component of total aircraft noise for the NASA Aircraft Noise Prediction Program (ANOPP). This Program is at Langley Research Center and is being developed jointly by various NASA centers with help from industry representatives. In the Program, the various contributors to and modifiers of aircraft noise are summed at various ground locations in order to predict a noise footprint for single- or multiple-event aircraft flights. The need for the ANOPP requires that this prediction method be based on the present state-of-the-art. Refined techniques and better data may be available in the near future to permit up-dating this prediction method. This report deals with noise generated by exhaust jets mixing with the surrounding air and does not consider other noises emanating from the engine exhaust, such as combustion and machinery noise generated inside the engine (i.e., core noise).

There have been a number of theoretical and empirical procedures developed to describe various aspects of jet noise. Most of these procedures have been based on the early theoretical work of Lighthill (refs. 1 and 2). He showed in reference 1 that the problem of sound generated by subsonic flows could be treated as a problem in classical acoustics, for which he then obtained a general solution. This solution was in terms of parameters which were not then, and still are not, directly measurable or readily determined from measurable data. Therefore, Lighthill used dimensional analysis to extract results of practical value from the theory. The major result was that the acoustic power should be proportional to $\rho_a V^8 c_a^{-5} l^2$, where ρ_a and c_a are

the ambient density and sonic velocity, respectively, V is the flow velocity, and l is a characteristic length (ref. 1). (Symbols are defined in appendix A.)

It has been well established that the energy source of jet noise is the turbulence created by the jet mixing with the surrounding air as Lighthill (ref. 2) suggested. Numerous attempts have been made to more fully quantify the nature of turbulence and then use this information to predict noise (e.g., refs. 3 to 12). These studies have had limited success, but have failed to produce a complete understanding of jet noise. In an engine, turbulence and velocity gradients upstream of the nozzle exit may significantly effect the nature of jet turbulence and therefore noise.

In addition to the acoustic power, the distribution of the sound in space (directivity) and its frequency content (spectra) are required to adequately describe and predict jet noise annoyance. Lighthill's theory (ref. 2), as supplemented by Ffowcs Williams (ref. 13), included the directivity of noise. According to this theory, the motion of the sound sources introduces a factor $(1 + M_c \cos \theta)^{-5}$ into the expression for the sound intensity, where M_c is the convection Mach number and is given by the velocity of the source (generally taken to be some fraction of the jet velocity) divided by the ambient speed of sound, and θ is the angle from the engine inlet axis. Ribner (ref. 14) treated the convection effect on directivity in a somewhat different manner. By allowing a somewhat different directionality for the noise directly generated by turbulence (self noise) and the noise due to the turbulence interacting with the mean flow (shear noise), he obtained a more complicated relation than reference 13. Goldstein and Howes (ref. 15) solved the convected wave equation and evaluated the source term using the isotropic turbulence model adopted by Lilley (ref. 7) and Ribner (ref. 16); the resulting directivity factor obtained is $(1 + M_c \cos \theta)^{-3}$, which has also been suggested by others. Recent data such as those of Olsen, Gutierrez, and Dorsch (ref. 17), Lush (ref. 18), and Krishnappa and Csanady (ref. 19) as well as those of Howes (ref. 20) support the

theory of Goldstein and Howes (ref. 15). However, because of refraction, none of these approaches accurately describes the observed noise directionality for hot jets or for cold jets near the jet axis. Local static temperature variations, which are present even in ambient total temperature jets, cause the sound rays to be refracted, or bent outward, away from the jet axis. The refraction effect increases with increasing frequency and temperature. There have been studies of this phenomenon (e.g., refs. 21 to 34), but the effect on jet noise has not yet been adequately described.

The frequency dependence of jet noise has generally been presented by plots of sound pressure level (SPL), normalized for the effects of size and jet velocity in some manner, against the Strouhal number, fD_e/V_j, for various angles. However, recent data (e.g., refs. 17, 18, and 35) show that near the jet axis the peak-SPL frequency is not affected by jet velocity, indicating that simple Strouhal-number scaling is not directly applicable, due to the effects of refraction.

Although there exists a lack of understanding of jet noise mechanisms, prediction methods have been proposed (e.g., refs. 35 to 39) based mainly on empirical treatment of the existing data. The predictions of Ahuja (ref. 35) and Olsen and Friedman (ref. 36) apply only to ambient temperature, subsonic jets. The SAE method (ref. 39) has been used widely, but its shortcomings are acknowledged and revision is being considered. However, the revised version is not yet available at this writing. References 36 to 39 include coaxial jets, and the method of Dunn and Peart (ref. 38) includes suppressor nozzles and ejectors. No published general methods are available for thrust reversers.

This report presents a first step toward the goal of developing a jet noise prediction method applicable to many types of exhaust systems of interest for aircraft. A goal of the interim method herein formulated is that it be capable of being modified easily for improvement as new information becomes available and existing information is more thoroughly analyzed.

Since convective amplification effects are minimized at 90^{o} to the jet axis, this angle was chosen as a baseline for developing the prediction method. First the overall sound pressure level is correlated at $\theta = 90^{o}$. Then the directivity in 1/3-octave bands is considered, and the spectra at various angles correlated, using the spectrum at $\theta = 90^{o}$ as a starting point.

The correlation is first developed for single, circular nozzles, starting with shock-free jets and no ambient velocity. The effects of shock noise and forward velocity are then considered. The methods are then extended and modified to include coaxial jets and noncircular jets. The method of Dunn and Peart (ref. 38) is proposed as an interim method for the the more complicated cases of suppressor nozzles and nozzles with ejectors. Although thrust reverser noise is not purely jet noise, it is included since it is generated by the exhaust stream outside the engine. Limited comparisons are made with other prediction methods and some of the available experimental data. A sample calculation is included to illustrate the prediction method.

APPROACH

The development of the recommended interim jet noise prediction method is described in this section. The formulation of this interim method is such that it can be easily modified and updated as new information becomes available. The noise levels are free-field (no reflections) referred to the source; that is, the effect of atmospheric absorption has been removed. Atmospheric attenuation effects are discussed in reference 40.

The geometric variables describing the position of the observer relative to the engine are sketched in figure 1. Since convective amplification effects are minimized at $\theta = 90^{o}$, this angle serves as a baseline for developing the prediction. The approach taken is described briefly as follows:

(a) The overall sound pressure level at $\theta = 90^{o}$, in normalized form, is first predicted as a function of jet velocity and other pertinent variables.

(b) The normalized sound pressure level spectrum is then predicted at $\theta = 90^{o}$.

(c) Then the directivity in normalized 1/3-octave bands is considered, and the spectra at various angles obtained.

The prediction is first developed for single, circular nozzles, starting with shock-free jets having no ambient velocity. The effects of shock noise and forward velocity are then considered. The prediction is next extended and modified to include coaxial jets, plug nozzles, and slot nozzles. Further modifications required for suppressor nozzles and ejectors are also considered, and the prediction of Dunn and Peart (ref. 38) is recommended for interim use. Thrust reverser noise prediction is included because it is generated by the exhaust outside the engine, even though it is not pure jet mixing noise.

Lighthill's analysis (refs. 1 and 2) established that the acoustic power for a jet is proportional to $\rho V_j^8 c_a^{-5} l^2$. If we take the characteristic dimension l to be the square root of the fully expanded jet area A_j, the intensity I at a distance R from the source would be given at $\theta = 90^{o}$ by

$$I = K_I \left(\frac{\rho V_j^8 A_j}{c_a^5 R^2} \right) \tag{1}$$

Where K_I is an experimentally determined coefficient, which might be correlated for various nozzle types and operating conditions.

In experiments, however, it is generally the mean-square pressure fluctuation, $\overline{p^2}$, which is measured and not the intensity. This mean-square pressure fluctuation is given by $I\rho_a c_a$, so

$$\overline{p^2} = K_I\left(\frac{\rho_a \rho V_j^8 A_j}{c_a^4 R^2}\right) \tag{2}$$

The rms pressure fluctuations are usually expressed in decibels referred to a reference pressure, p_{ref}, and physical properties are often referred to those for the International Standard Atmosphere (ISA). So an equivalent relation to equation (2) can be written in dimensionless logarithmic terms:

$$\text{OASPL} = 10 \log\left(\frac{\overline{p^2}}{p_{ref}^2}\right) = 10 \log\left(\frac{K_I \rho_{ISA}^2 c_{ISA}^4}{p_{ref}^2}\right) + 10 \log\left(\frac{V_j}{c_a}\right)^8 + 10 \log\left(\frac{A_j \rho_a \rho c_a^4}{R^2 \rho_{ISA}^2 c_{ISA}^4}\right) \tag{3}$$

So far in the present development no distinction has been made between the ambient density and the jet density in the sound intensity term. There is considerable disagreement in the literature on the proper method of accounting for the effect of jet density on noise. On the basis of data then available, von Glahn (ref. 41) found that the jet density had no effect on subsonic jet sound power levels and maximum sideline OASPL for jet total temperature from ambient to 1370 K (2460° R). This result was based on the data of references 42 to 47 and previously unpublished NASA hot jet data. In contrast, more recent results (refs. 38, 39, and 48 to 50) indicate that if the ambient density is used in equation (3), a term $10 \log\left(\frac{\rho_j}{\rho_a}\right)^w$ should be added to the right-hand side of the equation, where ρ_j is the fully-expanded jet density.

References 38, 48, and 49 indicate that the exponent w varies from about -1 to 0 at low subsonic velocities to about 2 at high supersonic velocities. The recent theories of Tanna, Fisher, and Dean (ref. 50) and Morfey (ref. 51) predict that an additional noise source due to temperature fluctuations in the shear layer could produce these apparent density effects. Although the subject of jet density or temperature effects requires further study, for the interim prediction method the following relation has been developed:

$$w = \frac{3(V_j/c_a)^{3.5}}{0.60 + (V_j/c_a)^{3.5}} - 1 \tag{4}$$

This expression is in reasonable agreement with references 38, 48, and 49. However, it is hoped that more fundamentally based methods of predicting the effect of ρ_j can be found. Incorporating this relation, the OASPL at $\theta = 90^o$ for simpler jets (nonsuppressors) will be correlated in the form,

$$OASPL_{90^o} - 10 \log\left[\left(\frac{A_j}{R^2}\right)\left(\frac{\rho_a}{\rho_{ISA}}\right)^2\left(\frac{c_a}{c_{ISA}}\right)^4\right] - 10\left[\frac{3(V_j/c_a)^{3.5}}{0.60 + (V_j/c_a)^{3.5}} - 1\right]\log\left(\frac{\rho_j}{\rho_a}\right) = K + 10 \log\left[\frac{(V_j/c_a)^a}{1 + b(V_j/c_a)^{a-3}}\right] \tag{5}$$

wherein the more complicated velocity term is so formulated to yield a third-power relation at very high velocities as in reference 41. (There are also theoretically based formulations giving similar results.) The constants a and b are determined for each type of configuration and K is in some cases a function of jet flow parameters, as well as geometry.

CIRCULAR NOZZLES

Overall Sound Pressure Level

The normalized overall sound pressure level at $\theta = 90^{\circ}$, $OASPL_{90^{\circ}}$

$$-10 \log\left[\left(\frac{A_j}{R^2}\right)\left(\frac{\rho_a}{\rho_{ISA}}\right)^2\left(\frac{c_a}{c_{ISA}}\right)^4\right] - 10\left[\frac{3(V_j/c_a)^{3.5}}{0.60 + (V_j/c_a)^{3.5}} - 1\right]\log\left(\frac{\rho_j}{\rho_a}\right),$$

is plotted against the jet velocity parameter, V_j/c_a, for shock-free circular jets in figure 2. The ambient jet temperature data are for jets ranging from 5.08- to 15.2-centimeter (2.0- to 6.0-in.) in diameter (refs. 17, 52, and 53). The hot jet data for a 38.1-centimeter (15.0-in.) diameter nozzle at temperatures from 700 to 1588 K (1260 to 2860° R) are partially from reference 41 and partially from previously unpublished NASA data; the test rig is described in references 41 and 54. There are considerably more data which should be considered in improving the prediction method (e.g., refs. 18 to 20, 42 to 45, 48, 50, and 55 to 58). However, it is of interest to note that Olsen, Gutierrez, and Dorsch (ref. 17) show their data to be in substantial agreement with those of Lush (ref. 18) for a 2.5-centimeter- (0.98-in.-) diameter jet. Predicted curves from Ahuja (ref. 35) and from Dunn and Peart (ref. 38) are also shown. Ahuja's prediction for ambient temperature jets (ref. 35) is in good agreement with the data of figure 2, but is applicable

only for $\rho_j \approx \rho_a$ and $V_j/c_a < 1.0$. The prediction of Dunn and Peart (ref. 38) does not agree with the data of figure 2, with the disagreement minimized around $V_j/c_a = 1.0$.

All of the data fall within ±3 dB of the recommended relation, which is given by equation (5) with $K = 141$, $a = 7.5$, and $b = 0.010$; that is

$$\mathrm{OASPL}_{90^o} - 10 \log \left[\left(\frac{A_j}{R^2} \right) \left(\frac{\rho_a}{\rho_{ISA}} \right)^2 \left(\frac{c_a}{c_{ISA}} \right)^4 \right] - 10 \left[\frac{3(V_j/c_a)^{3.5}}{0.60 + (V_j/c_a)^{3.5}} - 1 \right] \log \left(\frac{\rho_j}{\rho_a} \right) = 141 + 10 \log \left[\frac{(V_j/c_a)^{7.5}}{1 + 0.010\,(V_j/c_a)^{4.5}} \right] \qquad (6)$$

The value of a equal to 7.5 instead of 8, as expected from theory, is a consequence of the manner in which jet density (or temperature) effects are correlated; if w is set to 0 the eighth power relation is obtained for near-ambient temperature jets, but the effects of temperature are not correlated. Available experimental data for lower velocities are believed to be contaminated by internal noises, but for pure jet noise it is recommended that equation (6) be used. All of the data shown are for $M_j < 1.0$; however, the relations are recommended for fully expanded, shock-free supersonic jets as well.

SPL Spectra

The normalized sound pressure level spectrum at $\theta = 90^o$ is compared with data for shock-free circular jets in figure 3 for jet total temperatures

up to 1588 K (2860° R). The effect of jet temperature on the spectral shape is accounted for by multiplying the Strouhal number by the ratio of jet total temperature to ambient temperature to the 0.4 power, to give the nondimensional frequency parameter

$$S = \left(\frac{fD_e}{V_j}\right)\left(\frac{T_j}{T_a}\right)^{0.4} \tag{7}$$

For as much as 10 dB below the peak, more than 99 percent of the cold jet data are within ±2 dB of the recommended curve. Although the scatter is greater for the hot jets (primarily because hot jet experiments are difficult to perform accurately), the hot jet data do give a reasonable verification of the prediction method for jet total temperatures up to 1588 K (2860° R). A significant consideration is that at the higher frequencies, data are affected more by atmospheric absorption than are lower frequencies, and there is considerable disagreement on the magnitude of this effect. This uncertainty might effect the high-frequency roll-off, but not the OASPL. Worth considering in improving the prediction method might be (a) the use of fully expanded jet static temperature instead of total temperature, and (b) an exponent of 0.5 instead of 0.4; perhaps the observed effects might then be relatable to physical properties, such as jet sonic velocity, which varies with the square root of jet static temperature.

Directivity

The effect of source convection on the noise directivity has been found to introduce a factor $(1 + M_c \cos\theta)^{-n}$ (refs. 2, 13, and 15), where M_c is a fraction of V_j/c_a. Goldstein and Howes (ref. 15) obtained $n = 3$ from their theoretical studies and suggest $M_c = 0.62\,(V_j/c_a)$ for M_c less than 1.0. For values of M_c greater than 1.0, the simple directivity term becomes infinite for some angles, which is not consistent with experimental data. To eliminate this singularity, the directivity term of reference 15

is modified to $\left[1 + (M_c \cos\theta)/\left(\sqrt[5]{1 + M_c^5}\right)\right]^{-3}$ There are also theoretically based methods of eliminating this singularity (e.g., ref. 14), and these should be considered in improving the prediction method. The effects of refraction have not been as well defined, but it seems reasonable that the relative effects of convection and refraction should change with changing frequency.

Figure 4 shows plots of SPL relative to $\theta = 90^\circ$ corrected for convection,

$$\text{SPL-SPL}_{90^\circ} + 30 \log \left[1 + M_c \left(1 + M_c^5\right)^{-1/5} \cos\theta\right]$$

against angle θ at constant Strouhal number for cold jets. Figure 4(a) is for Strohal number $fD_e/V_j \approx 0.16$, which is near the peak SPL at the angle of maximum OASPL, while figure 4(b) is for $fD_e/V_j \approx 1.0$, which corresponds to the peak SPL at $\theta = 90^\circ$. It can be seen that for θ from about 60° to 120°, the convection relation fits the data rather well (zero value). This agreement is also observed for other Strouhal numbers and, therefore, for the OASPL. At angles near the jet axis, the data deviate significantly from a simple convection relation. This is probably due to refraction, but may also be a function of the relative magnitudes of shear noise and self noise.

In order to account for the experimentally obtained spectral directivities, empirically determined adjustments were established to the directional relations indicated by simple convection effects. Figure 5 gives the results of this matching process. The ordinate is

$$\text{SPL-OASPL}_{90^\circ} + 30 \log \left[1 + M_c \left(1 + M_c^5\right)^{-1/5} \cos\theta\right]$$

which for the simple convective model would fully account for the directivity effects. The abscissa is a modified Strouhal number defined by

$$S = \left(\frac{fD_e}{V_j}\right)\left(\frac{T_j}{T_a}\right)^{0.4(1+\cos\theta')} \tag{8}$$

Where the effective angle θ' is given by

$$\theta' = \theta\left(\frac{V_j}{c_a}\right)^{0.1} \tag{9}$$

Figure 5 contains a family of curves, each of which applies for a given constant value of the effective angle θ'. The variation of the effect of temperature with angle, as accounted for by the abscissa in figure 5 can be related to refraction effects. Since higher frequencies are more strongly effected by refraction (due to their relatively short wavelength), the high frequencies are increased relative to the lows away from the jet axis, and this effect increases with increasing jet temperature. At angles near the jet axis the low frequencies dominate since the highs have been refracted outward, and these low frequencies are relatively unaffected by refraction, and hence are less sensitive to changes in jet temperature. For $\theta' \leq 110^{\circ}$, the simple convection model is sufficiently accurate that a single curve is recommended. Any inaccuracy at small angles would be relatively unimportant anyway, since the noise levels are low, and on an airplane, other noise sources would generally be dominant in this sector. In the use of the recommended curves of normalized spectra against log S in figure 5 (given in 10° increments), linear logarithmic interpolation (and extrapolation, if required) is recommended.

Figure 6 illustrates the scatter involved in developing the curves in figure 5. For some of the data used in developing figure 5, experimental and calculated spectra are compared at an angle near the peak OASPL($\theta = 140^{\circ}$ to 145°) and at an angle between $\theta = 90^{\circ}$ and the peak.

Cases of a cold jet (fig. 6(a)) and a hot jet (fig. 6(b)) are considered. In all cases the region near the peak-SPL frequency is predicted fairly well. The data scatter at low frequency in figure 6(a) and at high frequency in figure 6(b) is due in part to inadequate corrections for ground reflections. As discussed previously, the high-frequency "roll-off" is an area requiring further study.

Supersonic Jets with Shock Noise

With underexpanded supersonic jets, especially at low jet temperatures, broadband shock noise is a significant problem and can dominate over jet noise. Discrete (narrow band) tones, generally termed "screech", are also often observed, but the present report will not treat this problem since such tones can often be eliminated by slight design modifications. Broadband shock noise has been the subject of several studies (e.g., refs. 4, 41, 42, 48, and 59 to 61). The approach used herein is that of von Glahn (ref. 41), who correlated the total overall sound power for underexpanded supersonic jets, $M_j \geq 1$, as follows:

$$W = 3.5 \times 10^{-3} F \rho_a A_j V_j^8 c_a^{-5} \Big/ \left[116.7 + (V_j/c_a)^8 M_j^{-3}\right] \qquad (10)$$

where F is a complicated function of jet Mach number, V_j and c_a. The shock noise tends to be more uniform in its directivity than jet noise, so as an approximation for this interim method it is taken to be uniform. The average OASPL obtained from equation (10) is modified to give only the shock noise component and assumed to hold for all angles; it is given as follows:

$$\overline{OASPL_s} - 10 \log\left[\left(\frac{A_j}{R^2}\right)\left(\frac{\rho_a}{\rho_{ISA}}\right)^2\left(\frac{c_a}{c_{ISA}}\right)^4\right] = 147 + 10 \log$$

$$\times\left\{\frac{12.5(M_j - 1)^3\left(\frac{V_j}{c_a}\right)^8}{\left[0.040 + (M_j - 1)^3\right]\left[1 + 2(M_j - 1)^4\right]\left[1 + 0.050\left(\frac{V_j}{c_a}\right)^8 M_j^{-3}\right]\left[1 + 0.0086\, M_j^{-3}\left(\frac{V_j}{c_a}\right)^8\right]}\right\} \qquad (11)$$

where $M_j > 1.0$. Also as an approximation for the iterim method, the normalized shock noise spectra at all angles are assumed to be the same as the jet mixing spectrum at $\theta = 90^0$ (fig. 7).

The shock noise spectrum obtained from figure 7 and equation (11) should then be added antilogarithmically to the jet mixing noise spectrum calculated for each angle from figure 5 and equation (6) to get the total spectrum for each angle.

Effects of Forward Velocity

It has been observed in model tests that forward velocity reduces jet noise at constant jet velocity. This noise reduction has been verified by comparisons of noise measurements from aircraft flyovers with static ground measurements (refs. 62 to 65). Such a reduction has been theoretically predicted by Ffowcs Williams (ref. 66), who suggested that the subsonic jet noise intensity should be proportional to $(V_j - V_o)^7 V_j$. The effects of forward velocity can be considered in two parts:

(a) The effect of the external flow field around the nozzle

(b) The effect of nozzle motion with respect to a stationary observer, commonly referred to as the Doppler effect.

Shock-free jets. - The effect of the external flow field can be simulated by placing the test nozzle in a wind tunnel or free jet. Recent tests of small nozzles in a large-diameter free jet (ref. 67) have shown that the acoustic intensity for a shock-free circular nozzle appears to be proportional to $(V_j - V_a)^6 V_j^2$, where V_a is the velocity of the ambient airflow with respect to the nozzle. Large-area-ratio coaxial nozzle tests show similar results. At $\theta = 90^o$, there is no Doppler effect, so the relative velocity dependency can be incorporated into equation (6) replacing V_j with $V_j(1 - V_a/V_j)^{3/4}$,

$$OASPL_{90^o} - 10 \log\left[\left(\frac{A_j}{R^2}\right)\left(\frac{\rho_a}{\rho_{ISA}}\right)^2\left(\frac{c_a}{c_{ISA}}\right)^4\right] - 10\left\{\frac{3\left[\left(\frac{V_j}{c_a}\right)\left(1 - \frac{V_a}{V_j}\right)^{3/4}\right]^{3/5}}{0.60 + \left[\left(\frac{V_j}{c_a}\right)\left(1 - \frac{V_a}{V_j}\right)^{3/4}\right]^{3.5}} - 1\right\}$$

$$\times \log\left(\frac{\rho_j}{\rho_a}\right) = 141 + 10 \log\left\{\frac{\left[\left(\frac{V_j}{c_a}\right)\left(1 - \frac{V_a}{V_j}\right)^{3/4}\right]^{7.5}}{1 + 0.010\left[\left(\frac{V_j}{c_a}\right)\left(1 - \frac{V_a}{V_j}\right)^{3/4}\right]^{4.5}}\right\} \qquad (12)$$

Note that it is assumed that the density exponent is also a function of the effective velocity, $V_j(1 - V_a/V_j)$. Equation (12) contrasts with earlier predictions (e.g., refs. 38 and 39) which replace V_j by $(V_j - V_a)$.

In reference 67, no frequency shifts at $\theta = 90^{o}$ were observed due to the ambient airflow. To include the effect of nozzle motion, the frequency should be Doppler shifted, as follows:

$$S = \left(\frac{fD_e}{V_j}\right) \frac{(T_j/T_a)^{0.4(1+\cos\theta')}}{\left[1 + (V_0/c_a)\cos\theta\right]} \tag{13}$$

The effect of motion on levels is included in the directivity plots of figure 5 by basing the convection Mach number on relative velocity,

$$M_c = 0.62(V_j - V_0)/c_a \tag{14}$$

It is assumed that the effective angle θ' is still given by equation (9).

Supersonic jets with shock noise. - For the interim prediction method it is assumed that shock noise is not effected by the external flow field. Simple Doppler corrections based on aircraft velocity are recommended. The OASPL should be shifted by

$$\Delta OASPL = 10 \log\left[1 + \left(\frac{V_o}{c_a}\right)\cos\theta\right] \tag{15}$$

and the frequency should be shifted, using equation (13). Figure 7 should then be used with these corrected OASPL and S values for each angle.

SIMPLE NONCIRCULAR NOZZLES

Plug Nozzles

Conical plugs (fig. 8) are sometimes used with circular nozzles. Limited data for such configurations have been reported in reference 17. The plug nozzles showed slightly lower noise levels than a circular nozzle of the

same cross-sectional flow area. It seems reasonable that a tapered plug could help decelerate the exhaust jet with reduced shear between the jet and the surrounding air, with a corresponding reduction in noise Therefore, to predict jet noise for a plug nozzle, equation (6) is simply modified to include the effects shown in reference 17, that is, by setting $K = 141 + 3 \log \left[0.10 + 2(h/D)\right]$, where h is the gap height and D is the circular nozzle diameter at the nozzle exit (fig. 8). In addition, it is reasonable to assume that this slightly modified relation would also hold with forward velocity. Thus, for a shock-free plug nozzle,

$$\mathrm{OASPL}_{90^o} - 10 \log \left[\left(\frac{A_j}{R^2}\right)\left(\frac{\rho_a}{\rho_{ISA}}\right)^2\left(\frac{c_a}{c_{ISA}}\right)^4\right] - 10\left\{\frac{3\left[\left(\frac{V_j}{c_a}\right)\left(1-\frac{V_a}{V_j}\right)^{3/4}\right]^{3.5}}{0.60+\left[\left(\frac{V_j}{c_a}\right)\left(1-\frac{V_a}{V_j}\right)^{3/4}\right]^{3.5}} - 1\right\}$$

$$\times \log\left(\frac{\rho_j}{\rho_a}\right) = 141 + 3 \log\left(0.10 + 2\,\frac{h}{D}\right) + 10 \log\left\{\frac{\left[\left(\frac{V_j}{c_a}\right)\left(1-\frac{V_a}{V_j}\right)^{3/4}\right]^{7.5}}{1+0.010\left[\left(\frac{V_j}{c_a}\right)\left(1-\frac{V_a}{V_j}\right)^{3/4}\right]^{4.5}}\right\} \tag{16}$$

The spectral effects observed in reference 17 were also slight except for very small annular gaps. It was found that the effects on SPL spectra can be roughly accounted for by multiplying the frequency by $(D_h/D_e)^{0.4}$ in the Strouhal number. No effect on directivity was reported. Hence, the

circular nozzle relations (fig. 5) should be used for plug nozzles with S redefined as follows:

$$S = \frac{fD_e(D_h/D_e)^{0.4}(T_j/T_a)^{0.4(1+\cos\theta')}}{V_j\left[1 + (V_o/c_a)\cos\theta\right]} \tag{17}$$

It should be noted that these plug nozzle relations are preliminary in nature. However, for practical-type geometries, it is expected that the effects of the plug on jet noise would be rather small. There are no data on the effect of the plug on supersonic jets with shock noise, so for the interim method, the plug nozzle is treated the same as the circular supersonic nozzle jet of the same flow area.

Slot Nozzles

Slot nozzles are considered herein since they are being considered for powered-lift systems, such as the augmentor wing concept for STOL aircraft and for possible advanced supersonic transport applications.

Overall sound pressure level at $\theta = 90^\circ$. - Cold flow test data are available for slot nozzles having aspect ratios of 4.8 (refs. 68 and 69) and 69 (refs. 17 and 70) at various azimuthal angles φ. Since the jet is not axisymmetric, some effect of φ might be expected. (The slot nozzle long dimension lies in the $\varphi = 90^\circ$ direction (fig. 1).) For these geometries, the OASPL data show reasonably good agreement with the circular nozzle prediction relations (eq. (6)) for shock-free jets, as shown in figure 9. It is also assumed that the circular nozzle forward velocity and shock noise effects apply. Hence, equation (12) for shock-free jets and equations (11) and (16) with shock noise are recommended, and the slight effect of φ can be neglected. Other data which might be applicable, but were not included because of time constraints, may be found in references 71 to 73.

SPL spectra and directivity. - Normalized SPL spectra at $\theta = 90^{\circ}$ for the slot nozzles of references 17 and 68 to 70 are shown in figure 10 for azimuthal angles φ of 0°, 45°, and 90°. For $\varphi = 0^{\circ}$ (fig. 10(a)) and $\varphi = 45^{\circ}$ (fig. 10(b)) the normalized spectra agree with those of the circular nozzle on the basis of a modified Strouhal number, like that used for plug nozzles (eq. (17)). The relative velocity and temperature effects previously given for the circular nozzle are assumed to also apply to the slot nozzle. Figure 10(c), for $\varphi = 90^{\circ}$, indicates a much poorer agreement with the circular nozzle curves especially at the lower frequencies. This poor agreement could be due to the small characteristic dimension or to the anisotropic nature of the turbulence, but could also be due in part to the ground reflection effects in these particular experimental data. Although there are some additional effects, due probably to the nonisotropic nature of the turbulence, for the slot nozzle at large polar angles θ, the directional effects are close enough to those for the circular nozzle (fig. 5), so that the circular nozzle relations are recommended for use in slot nozzle noise prediction with the use of S from equation (17).

COAXIAL NOZZLES

Olsen and Friedman (ref. 36) have correlated shock-free cold coaxial jet noise data for secondary-to-primary jet velocity ratios, $V_{j,2}/V_{j,1}$, from 0.2 to 1 and secondary-to-primary area ratios, $A_{j,2}/A_{j,1}$, from 0.67 to 43.5. This correlation (ref. 36) is based on extension and modification of the method of Williams, et al (ref. 74). The method of reference 36 is herein modified and extended to account for the case of a heated, shock-free primary jet, taking into consideration the data of Eldred, et al (ref. 75). The approach used is as follows: (1) The OASPL and the spectra at $\theta = 90^{\circ}$ are related to those of the core jet alone (either circular nozzle or plug nozzle) by means of simple correlation factors, and (2) the directivity relative to $\theta = 90^{\circ}$ is taken to be the same as for the core jet alone, as the experiments had indicated. Olsen and Friedman (ref. 36)

found no significant differences when the core nozzle was extended beyond the secondary nozzle exit. For an extended secondary duct the problem becomes more complicated and needs study, but the method presented herein is recommended as an interim prediction. Few experiments on the cases of a heated secondary flow and of $V_{j,2}/V_{j,1} > 1$ have been reported, so although the relations developed herein are recommended as an interin method, they should be considered preliminary and unproven for these cases.

Overall Sound Pressure Level

The effects of area ratio, velocity ratio, and temperature ratio are shown in figure 11, where the OASPL relative to that of the core jet alone, corrected for temperature ratio,

$$OASPL_{90^o} - OASPL_{90^o,1} - 10 \log \sqrt{\frac{T_{j,1}}{T_{j,2}}}$$

is plotted against area ratio for various velocity ratios. The temperature ratio term is an interim approximation. The curves shown correspond to the recommended relation (slightly modified from ref. 36),

$$OASPL_{90^o} - OASPL_{90^o,1} = 5 \log\left(\frac{T_{j,1}}{T_{j,2}}\right) + 10 \log\left[\left(1 - \frac{V_{j,2}}{V_{j,1}}\right)^m + 1.2 \frac{\left(1 + \frac{A_{j,2} V_{j,2}^2}{A_{j,1} V_{j,1}^2}\right)^4}{\left(1 + \frac{A_{j,2}}{A_{j,1}}\right)^3}\right] \tag{18}$$

In equation (18), $OASPL_{90^o,1}$ is the OASPL at $\theta = 90^o$ for the core jet alone, from equation (12) for a circular core nozzle or equation (16) for a plug core

nozzle. (According to ref. 67, the effect of forward velocity on the OASPL should be the same as for a single circular nozzle.) The exponent m is given by

$$\left.\begin{aligned} m &= 1.1\sqrt{\frac{A_{j,2}}{A_{j,1}}} \quad ; \quad \frac{A_{j,2}}{A_{j,1}} < 29.7 \\ m &= 6.0 \quad ; \quad \frac{A_{j,2}}{A_{j,1}} \geq 29.7 \end{aligned}\right\} \tag{19}$$

The ambient temperature data of reference 36 are within approximately ±2 dB of the curves shown, with the greatest scatter at a velocity ratio, $V_{j,2}/V_{j,1}$, of about 0.6.

SPL Spectra

The shapes of the SPL spectra for shock-free coaxial jets were generally found in reference 36 to be the same as for a circular nozzle, but with the frequencies shifted. Figure 12 shows the effect of area ratio and velocity ratio on the frequency shift parameter,

$$F_S = \left(1 - \frac{S_1}{S}\right)\left(\frac{T_{j,1}}{T_{j,2}}\right) \tag{20}$$

where S_1 is the effective Strouhal number for the core nozzle alone, whether a plug or circular core nozzle, and the temperature ratio term is an interim approximation. Limited data (one value of $V_{j,1}/V_{j,2}$) from reference 67 indicates that with or without forward velocity, the primary jet velocity should be used in the Strouhal number. Thus equation (17) using core jet parameters is recommended for this interim method.

The recommended curves in figure 12 are based on the ambient temperature data of reference 36 at $\theta = 90^{o}$ and $V_{j,1}/c_a \approx 0.87$; however, data for other polar angles and core jet velocities show similar trends. These data scatter within a frequency range of ±one 1/3-octave band from the curves, except at a velocity ratio, $V_{j,2}/V_{j,1}$, of 0.4 for area ratios, $A_{j,2}/A_{j,1}$, above 16, where double-peaked spectra occurred; however, area ratios that high are of little practical interest.

Supersonic Jets with Shock Noise

Dosanjh and associates (refs. 76 to 78) have reported that for supersonic secondary flows, large noise reductions compared to the secondary jet alone are obtained when the primary jet velocity reaches a critical value in the supersonic range. These reductions are attributed to changes in the shock structure. However, a significant amount of the reduction appears to be due to the elimination of narrowband noises. Due to the limited nature of these tests (refs. 76 to 78), the only supersonic effects included in the recommended interim method are those outlined in the following paragraphs, which are purely arbitrary.

Supersonic primary with subsonic secondary. - When the primary jet is not fully expanded (shocks present), equations (11) and (15) are used to determine the primary jet shock noise level. Equation (20) is then used to adjust this level to the coaxial nozzle noise level, as described earlier. The shock noise spectra are then obtained from figure 7 with S from equations (20) and (17). The shock noise spectrum is then added antilogarithmically to the jet noise spectrum.

Supersonic secondary. - For a supersonic secondary it is recommended, as an interim approximation, to calculate the noise of the secondary stream alone, as if the core nozzle were replaced by a plug. Then the noise for the core nozzle alone should be calculated, whether subsonic or supersonic, and then these levels added antilogarithmically. This probably will give a conservatively high noise estimate, since there may be interaction effects present which would reduce the noise.

SUPPRESSOR NOZZLES

Because jet noise is a major problem for turbojet and low-bypass turbofan engines, various types of noise-suppression nozzle systems have been developed. A number of such systems have been developed, having considerably different noise characteristics. Suppressor nozzles generally consist of multiple tubes (refs. 55 and 79 to 86) or multiple lobes (refs. 64, 65, 86, 87, and 88); nozzles of these types can also be used to promote rapid jet velocity decay for blown flap powered-lift systems (refs. 67, 89, and 90). Many problems remain to be solved in order to obtain accurate means of predicting suppressor nozzle noise; however, since it is necessary to make noise predictions at present, the prediction of reference 38 is recommended as an interim method.

For purposes of jet noise correlation and prediction, the noise from a multielement nozzle is typically considered to consist of two parts. Reference 38 terms these premerging noise and postmerging noise. The premerging noise is taken to be that generated near the nozzle where the structure of the individual jet elements can still be identified. The postmerging noise is taken to be that generated further downstream of the nozzle after the individual jet elements and the entrained airflow have effectively merged into a single jet of lower velocity. The higher frequencies are dominated by the premerging noise, and the lower frequencies are dominated by the postmerging noise. Reference 38 presents methods of predicting these two noise spectra; the spectra obtained are then summed antilogarithmically to obtain the total spectrum. A typical example for a YJ 75 engine with a 37-tube nozzle is shown in figure 13 (from ref. 38).

In conjunction with multitube or multilobe nozzles, ejectors are also used in some suppressor systems (e.g., see refs. 55 and 79). The ejector modifies both the jet mixing and the noise generation. Acoustic lining is often used to absorb some of the premerging noise generated near the nozzle exit, generally at relatively high frequencies. In the case of a multitube nozzle, the noise generated by the individual jets

(premerging) might be largely eliminated as illustrated in figure 13 as an example.

The recommended method for suppressors from reference 38 is repeated herein in appendix B (essentially verbatim) using the nomenclature of this study. This prediction procedure is essentially empirical It gives free-field, far-field spectra at R = 1 m (3.28 ft) from the source. It is based on data from round nozzles and suppressor nozzles for the following types of tests:

1. Full-scale JT8D, JT3C, JT4/J75, and JT12 static engine tests.
2. Model scale hot flow tests ($A_j \approx 0.0046$ m^2 ($\sim$0.049 ft^2)).
3. Flight tests of 707, 727, and 737 airplanes.

THRUST REVERSERS

Thrust reversal is used to shorten the landing distance for both conventional (CTOL) and reduced- or short-takeoff-and-landing (RTOL and STOL) aircraft. In addition, augmentor-wing-type STOL or RTOL airplanes may use core jet thrust reversal to steepen the approach flight path. In the interests of minimizing the noise associated with aircraft operations, all potential noise sources should be considered, and until recently thrust reverser noise has received little attention.

The NASA Lewis Research Center has initiated studies of thrust reverser noise (refs. 68, 70, and 91 to 93). Target-type reversers (fig. 14) were used in the earliest tests because of their simplicity and because they can reverse both circular nozzle (refs. 91 and 92) and slot nozzle (refs. 68 and 70) flows. More recently, cascade-type reversers (fig. 15) have also been tested (ref. 93). All of these experiments were performed with ambient temperature jets. Reverse-pitch fans are also being considered for thrust reversal, but are not included herein.

Reverser noise should be treated as the sum of a modified jet noise and jet-surface interaction noise, but for the present these noise sources will not be separated. Generally, the jet-surface interaction noise is dominant over the frequency range of interest except for some cascade

reverser configurations at high jet velocities. The spectral shapes do not change much with angle, again with the exception of some cascade reversers at high V_j. Therefore, the overall directivity and the space-averaged SPL spectra are recommended, and the effect of relative velocity is assumed to be negligible for the interim prediction method.

Target-Type Reversers

OASPL at $\theta = 90^\circ$ - The normalized OASPL at $\theta = 90^\circ$ is plotted against log (V_j/c_a) in figure 16 for the various semicylindrical and V-gutter reversers tested. A simple density effect (w = 1) is assumed for reversers. It is quite apparent that the reversers significantly increase the noise levels above the jet noise curve (eq. (6) with $\rho_j = \rho_a$). The variation of reverser noise with jet velocity is less than for jet noise, so the difference between the reverser noise and jet noise increases with decreasing velocity. The V-gutter reversers are somewhat noisier than the semicylindrical reversers, except that for the large-aspect-ratio V-gutter there is a significant noise reduction in the $\varphi = 90^\circ$ plane. The recommended relation for the target reverser OASPL at $\theta = 90^\circ$ is given as follows:

$$\mathrm{OASPL}_{90^\circ} - 10 \log \left(\frac{A_j \rho_j \rho_a c_a^4}{R^2 \rho_{ISA}^2 c_{ISA}^4} \right) = K_r - 10 \cos^2 \varphi \log \left(\frac{D_h}{D_e} \right) + 10 \log \left[\frac{\left(\frac{V_j}{c_a} \right)^{5.5}}{1 + 0.010 \left(\frac{V_j}{c_a} \right)^{2.5}} \right] \qquad (21)$$

where $K_r = 149$ for the semicylindrical reversers and 154 for the V-gutters. The velocity effect is arbitrarily formulated to yield a V_j^3 relation at high velocities like pure jet noise.

Directivity. - Reference 94 presents a correlation which predicts the OASPL directivity for the semicylindrical reversers of reference 91 reasonably well. There are deviations from this relation for the V-gutter reversers, but it is considered sufficiently accurate for the interim prediction method. Reference 94 gives OASPL $\propto 10 \log \left[\cos^2(\theta/3)\right]$, so for the interim method,

$$\text{OASPL} = \text{OASPL}_{90^o} + 20 \log \left[\frac{\cos\left(\frac{\theta}{3}\right)}{\cos 30^o} \right] \tag{22}$$

Spectra. - The normalized space-average SPL spectra shown in figure 17 are recommended for all angles. The same $(D_h/D_e)^{0.4}$ factor modifying the Strouhal number for slot nozzles also appears adequate for these reversers, so S is obtained from equation (17), using nozzle exit conditions. No other temperature effect is included since there are no data available on which to base a correction.

Cascade-Type Reversers

OASPL at $\theta = 90^o$. - The normalized OASPL at $\theta = 90^o$ is plotted against log (V_j/c_a) for the various cascade reversers tested in figure 18. Although the same trend of increased noise levels above jet noise is observed as for the target reversers, the magnitude of the increase is less. In order to account for the closeness of the quieter cascades to the jet noise curve, a two-step approach is recommended for the reverser noise calculation. First the additional noise due to thrust reversal over that due to the jet alone is correlated in a manner similar to equation (21), that is,

$$OASPL_{90^o,cr} = K_{cr} + 10 \log\left(\frac{A_j \rho_j \rho_a c_a^4}{R^2 \rho_{ISA}^2 c_{ISA}^4}\right) + 10 \log\left[\frac{\left(\frac{V_j}{c_a}\right)^5}{1 + 0.010\left(\frac{V_j}{c_a}\right)^2}\right] \quad (23)$$

where K_{cr} is obtained from the following:

$$K_{cr} = 136 + \Delta K_{cr,1} + \Delta K_{cr,2} + 7.2\left(\frac{A_e}{A_t}\right) \quad (24)$$

where

$\Delta K_{cr,1}$ = 0 if there is an internal flow deflector to guide the flow into the cascades, or

$\Delta K_{cr,1}$ = 5 if there is no deflector;

$\Delta K_{cr,2}$ = 0 if airfoil-shaped vanes are used, or

$\Delta K_{cr,2}$ = 6 if constant-thickness vanes are used;

A_e/A_t = is the cascade-exit-to-tailpipe area ratio (generally > 1.0)

This level is then added antilogarithmically to the jet noise calculated from equation (6) for the cascade exit conditions, $OASPL_{90^o,j}$, to get the OASPL,

$$OASPL_{90^o} = 10 \log\left[10^{(OASPL_{90^o,cr})/10} + 10^{(OASPL_{90^o,j})/10}\right] \quad (25)$$

Obviously, there is much improvement to be made in this interim method to eliminate the arbitrary correction factors.

Directivity. - The OASPL directivities of the various cascade reversers are complicated in shape, but relatively small in magnitude. These

patterns are represented for the present interim prediction by the approximate relation,

$$\text{OASPL} - \text{OASPL}_{90^o} = 20 \log\left[1 + \frac{1}{2}\sin(2\theta)\right] \tag{26}$$

Spectra. - The space-average SPL spectrum, recommended for use at all angles is shown in figure 19; again the $(D_h/D_e)^{0.4}$ factor is used to try to predict the relative effect of the total reverser area (D_e) and the individual passage size (D_h), so S is computed from equation (17).

SUMMARIZATION OF RECOMMENDED INTERIM PREDICTION METHOD

To facilitate calculations, the recommended prediction method is summarized in this section and in table I. Furthermore, an illustrative sample calculation is given in appendix C.

For circular and slot nozzles, equation (12) yields the OASPL at $\theta = 90^o$; for plug nozzles equation (16) is used. For each of these configurations, the SPL spectrum is then obtained from figure 5 with S from equation (17) and M_c from equation (14). If the jet is not fully expanded, shock noise is also present, and the shock noise is estimated from equations (11) and (15) for all nozzle shapes. The shock noise SPL spectrum is obtained from figure 7 with S from equation (17). The shock noise spectrum is then added antilogarithmically to the jet noise spectrum at each angle.

For coaxial nozzles the noise of the core jet alone is computed as described above, and correction factors are then applied. The noise levels are modified according to equations (18) and (19), and the frequencies shifted according to figure 12 and equation (20) with the core-jet Strouhal number based on $V_{j,1}$ (eq. (17)).

Prediction of thrust reverser noise is also included. The OASPL at $\theta = 90^o$ is computed from equation (21) for the target reversers and equa

tions (23), (24), and (25) for cascade reversers. The OASPL directivity is obtained from equation (22) or (26) for target or cascade reversers, respectively. The same spectral shapes are used in all directions, using a modified Strouhal number from equation (17); target reverser spectra are shown in figure 17 and the cascade reverser spectra in figure 19.

A new prediction method for suppressor nozzles with and without ejectors has not yet been obtained. Therefore, the methods of Dunn and Peart (ref 38), outlined in appendix B, for noise calculations for such systems is recommended

FURTHER RESEARCH REQUIREMENTS

Several important problems should be studied to produce a better understanding of jet noise mechanisms and thereby improve the methods of jet noise prediction. Most fundamentally, the knowledge of the jet turbulence structure and its relation to jet noise should be improved. This should allow for a better separation between the effects of convection and refraction and between shear noise and self noise. A better understanding of the locations of noise sources in the flow field would aid in the formulation of suppressor nozzle predictions, especially those with ejectors. The effect of turbulence entering the nozzle exit plane from upstream on noise production should be determined, and a means of predicting this effect should be developed if the problem is significant.

In areas of more applied research, there is still a need for experimental jet noise data at elevated jet temperatures, especially for coaxial nozzles and thrust reversers. Theoretical studies should be focussed on the effects of elevated temperature also, so that the variable-density-exponent correlation can be replaced by a more fundamentally based approach. Further studies of relative velocity effects are needed to verify and extend the results of reference 67 especially for suppressor nozzles and thrust reversers. Atmospheric absorption should be accurately determined at frequencies up to at least 100 kHz to increase the range available for model scale testing. The effect of installing nozzles

on airplanes near surfaces can cause increased low frequency noise; this problem should be further investigated.

The prediction method itself should be compared with all available pertinent data and modified, if necessary. The suppressor, shock noise, and reverser noise methods can probably be improved.

CONCLUDING REMARKS

This report presents an interim method of calculating the noise generated by the exhaust jet mixing with the surrounding air for circular, plug, slot, and coaxial nozzles. The effects of jet temperature, jet velocity, and vehicle forward speed are included as well as the effects of ambient conditions and the geometric variables. An existing prediction method is recommended for suppressor nozzle systems. An approximate prediction method for thrust reverser noise is also presented, not including the effects of variations in jet temperature and vehicle forward speed. Research which is critical to the improvement of these prediction methods is identified. It is intended that these methods be improved and updated as new information becomes available.

APPENDIX A

SYMBOLS

A	area, m^2 (ft^2)
A_{ref}	reference area, 0.0929 m^2 (1 ft^2)
a	exponent in equation (5), dimensionless
A_e	geometric exit area, m^2 (ft^2)
A_t	tailpipe area ahead of reverser, m^2 (ft^2)
b	coefficient in equation (5), dimensionless
c	speed of sound, m/sec (ft/sec)
D	circular nozzle diameter, m (ft)
D_e	equivalent circular nozzle diameter, $\sqrt{\frac{4A}{\pi}}$, m (ft)
D_h	hydraulic diameter, 4A/(perimenter), m (ft)
F	shock noise factor in equation (10), dimensionless
F_1	parameter defined in suppressor noise prediction (appendix B), dB re 20 $\mu N/m^2$
F_2	parameter defined in suppressor noise prediction (appendix B), dB re 20 $\mu N/m^2$
F_3	parameter defined in suppressor noise prediction (appendix B), dB re 20 $\mu N/m^2$
F_4	parameter defined in suppressor noise prediction (appendix B), dB re 20 $\mu N/m^2$
F_5	parameter defined in suppressor noise prediction (appendix B), dimensionless
F_6	parameter defined in suppressor noise prediction (appendix B), dB re 20 $\mu N/m^2$

F_7	parameter defined in suppressor noise prediction (appendix B), dB re 20 $\mu N/m^2$
F_8	parameter defined in suppressor noise prediction (appendix B), dB re 20 $\mu N/m^2$
F_9	parameter defined in suppressor noise prediction (appendix B), dimensionless
F_s	frequency shift parameter (eq. (2)), dimensionless
f	1/3-octave-band center frequency, Hz (cycles/sec)
f_o	reference frequency, Hz (cycles/sec)
h	plug nozzle annular gap height, m (ft)
I	acoustic intensity, W/m^2 (lb_f/ft-sec)
K	coefficient in equation (5), dB re 20 $\mu N/m^2$
K_{cr}	coefficient in equation (23), dB re 20 $\mu N/m^2$
$\Delta K_{cr,1}$	coefficient in equation (24), dB re 20 $\mu N/m^2$
$\Delta K_{cr,2}$	coefficient in equation (24), dB re 20 $\mu N/m^2$
K_I	coefficient in equation (1), dimensionless
K_r	coefficient in equation (21), dB re 20 $\mu N/m^2$
ℓ	characteristic dimension, m (ft)
M	Mach number, dimensionless
m	exponent in equation (18), dimensionless
M_c	convection Mach number, dimensionless
N	number of suppressor elements, dimensionless
n	convection parameter exponent, dimensionless
OASPL	overall sound pressure level, dB re 20 $\mu N/m^2$
$\overline{OASPL}$	space-average OASPL, dB re 20 $\mu N/m^2$

p_{ref}	reference pressure, 20 $\mu N/m^2$
$\overline{p^2}$	mean-square acoustic pressure fluctuation, N^2/m^4 (lb_f^2/ft^4)
R	distance from source to observer, m (ft)
R_A	ratio of exit flow area to base area, dimensionless
S	effective Strouhal number, dimensionless
SPL	1/3-octave-band sound pressure level, dB re 20 $\mu N/m^2$
T	total temperature, K (^oR)
T_s	static temperature, K (^oR)
$T_{s,ref}$	reference static temperature (fig. 22), K (^oR)
V	velocity, m/sec (ft/sec)
V_o	vehicle forward speed, m/sec (ft/sec)
V_R	effective relative velocity (eq. (B5)), m/sec (ft/sec)
W	sound power, W (lb_f-ft)
w	variable density exponent, dimensionless
ρ	density, kg/m^2 ($slugs/ft^3$)
ρ_{ref}	reference density, 16.02 kg/m^2 (0.0311 $slugs/ft^3$)
φ	azimuthal angle (fig. 1), deg
θ	polar angle from inlet (fig. 1), deg
θ'	effective polar angle from inlet, $\theta(V_j/c_a)^{0.1}$, deg

Subscripts:

1	core jet
2	fan (bypass) jet
a	ambient
cr	cascade reverser
j	jet (fully-expanded)

jm	mixed jet (ejector exit) mean value
ISA	international standard atmosphere, 288 K (519^{o} R) and 101.3 kN/m^2 (2120 lb_f/ft^2)
s	shock noise
90^{o}	parameter evaluated at $\theta = 90^{o}$

APPENDIX B

SUPPRESSOR NOISE PREDICTION

The recommended method for suppressors from reference 38 is repeated herein (essentially verbatim) using the nomenclature of this study. This prediction procedure is essentially empirical. It gives free-field, far-field spectra at R = 1 m (3.28 ft) from the source. It is based on data from round nozzles and suppressor nozzles for the following types of tests:

1. Full-scale JT8D, JT3C, JT4/J75, and JT12 static engine tests.
2. Model scale hot flow tests ($A_j \approx 0.0046$ m^2 ($\sim$0.049 ft^2)).
3. Flight tests of 707, 727, and 737 airplanes.

Postmerging Noise Prediction

Consider the ejector/suppressor configuration shown in figure 20. The postmerging noise for the ejector exhaust is assumed to be similar to that of a conventional circular jet. The OASPL for an engine is related to the relative jet velocity, density of the exhaust, static temperature, and discharge area, as follows:

$$\mathrm{OASPL}(\theta) = F_1(V_{jm} - V_o, \theta) + 10 \log \left[\left(\frac{\rho_{jm}}{\rho_{ref}} \right)^2 \left(\frac{T_{s,jm}}{T_{s,ref}} \right)^{1.5} \left(\frac{A_{jm}}{A_{ref}} \right) \right] \tag{B1}$$

where F_1 is obtained from figure 21, $T_{s,ref}$ from figure 22, ρ_{ref} is 16.02 kg/m^3 (0.0311 slugs/ft^3), and A_{ref} is 0.0929 m^2 (1 ft^2). The subscript jm refers to the mixed jet (ejector exhaust) mean, one-dimensional flow value.

The 1/3-octave-band SPL spectrum is calculated by adding the following corrections to the OASPL, that is,

$$SPL(f, \theta) = OASPL(\theta) + F_2\left(\frac{f}{f_o}\right) + F_3\left(\frac{f}{f_o}, \theta\right) \tag{B2}$$

where F_2 is obtained from figure 23, F_3 from figure 24, and f_o is a characteristic frequency given by $\left[\frac{V_j^2}{(V_j - V_o)D_{e,jm}}\right] F_4(V_j - V_o, \theta)$, with $D_{e,jm}$ the equivalent diameter of the ejector exhaust, and F_4 is from figure 25.

When the shroud (ejector) is removed, the one-dimensional flow parameters for the postmerging noise region are difficult to define. This problem has been avoided through the use of one-dimensional flow parameters for the suppressor exhaust. This approach resulted in an empirical correction term being added to equation (B1). The correction term is defined as a function of the area ratio R_A and relative velocity, that is,

$$\Delta OASPL = 0.34\left[F_5(V_j - V_o)\right]\sqrt{R_A - 1} \tag{B3}$$

where F_5 is obtained from figure 26. The "effective" one-dimensional flow values to use in equations (B1) and (B2) for no ejector are: $V_{jm} = V_j$, $\rho_{jm} = \rho_j$, $T_{s,jm} = T_{s,j}$ and $D_{e,jm} = D_e\sqrt{R_A}$.

Premerging Noise Prediction

Consider the "bare" suppressor configuration without ejector shroud. The premerging noise of a single element, tube, or lobe, etc., is assumed to be similar to that of a conventional circular jet of the same discharge area. However, the individual jets for the multielement suppressor interfere with each other and alter the turbulent structure (ref. 95). By dimensional analysis, the effects of the interferring jets have been related to the number of elements and the area ratio for the suppressor. From this analysis the space-average OASPL is defined empirically as

$$\overline{\text{OASPL}} = F_1(V_R,\ 120^\circ) + 10 \log\left[\left(\frac{\rho_j}{\rho_{ref}}\right)^2 \left(\frac{T_{s,j}}{T_{s,ref}}\right)^{1.5} \left(\frac{A_j}{A_{ref}}\right)\right]$$

$$+ F_6(N) + F_7(R_A) \qquad \text{(B4)}$$

where F_1 is obtained from figure 21, F_6 from figure 27, F_7 from figure 28, N is the number of elements, and R_A is the area ratio: base area divided by primary area. V_R is obtained from

$$\left.\begin{aligned} V_R &= V_j \text{ for ground static noise} \\ &= V_j - 0.04\, c_a \text{ in flight} \end{aligned}\right\} \qquad \text{(B5)}$$

The OASPL varies with the directivity angle θ, as follows:

$$\text{OASPL}(\theta) = \overline{\text{OASPL}} + F_8(\theta) \qquad \text{(B6)}$$

where F_8 is obtained from figure 29.

Finally, the 1/3-octave-band SPL spectrum is obtained in a manner similar to that of the postmerging noise, except that the characteristic frequency f_o is typically higher and an apparent 10° shift relative to the postmerging noise must be added to the directivity angle. That is,

$$\text{SPL}(f, \theta) = \text{OASPL}(\theta) + F_2\left(\frac{f}{f_o}\right) + F_3\left(\frac{f}{f_o},\ \theta + 10^\circ\right) \qquad \text{(B7)}$$

where F_2 is obtained from figure 23, F_3 from figure 24, and

$$f_o = \frac{V_j^2 \sqrt{N}}{V_R D_e} F_4(V_R, \theta) F_9(M_j) \tag{B8}$$

where F_4 is obtained from figure 25 and F_9 from figure 30.

When a hardwall shroud, less than 2.5 diameters long, is placed on the exhaust system, the performance of the configuration changes, and the induced secondary Mach number increases. For this short shroud, no apparent shielding takes place, and the premerging noise level has not been observed to change significantly. However, this should not be the case when the shroud is lined.

APPENDIX C

SAMPLE CALCULATION

To illustrate the use of this prediction method a sample problem is solved in this section. The stepwise outline of the calculations required for such predictions is given in figure 31. The problem chosen is to predict the jet noise free-field, far-field spectrum at a polar angle $\theta = 150^{o}$ and a distance $R = 30.5$ m (100 ft) from a coaxial nozzle whose core nozzle has a plug, with ambient conditions corresponding to the International Standard Atmosphere. (See fig. 8 for plug nozzle geometric variables.)

Given: plug nozzle gap height, $h = 0.150$ m (0.49 ft)

core nozzle diameter, $D = 0.744$ m (2.44 ft)

core jet area, $A_{j,1} = 0.279$ m^2 (3.00 ft^2)

fan jet area, $A_{j,2} = 0.948$ m^2 (10.20 ft^2)

core jet velocity, $V_{j,1} = 366$ m/sec (1200 ft/sec)(subsonic at $T_{s,j,1}$)

fan jet velocity, $V_{j,2} = 293$ m/sec (960 ft/sec)

airplane velocity (also ambient velocity, V_a) $V_o = 122$ m/sec (440 ft/sec)

core jet total temperature, $T_{j,1} = 700$ K (1260^{o} R)

fan jet total temperature, $T_{j,2} = 322$ K (580^{o} R)

fully expanded core jet density, $\rho_{j,1} = 0.561$ kg/m^3 (0.00109 slugs/ft^3)

fully expanded fan jet density, $\rho_{j,2} = 1.21$ kg/m^3 (0.00233 slugs/ft^3)

ambient density, $\rho_a = \rho_{ISA} = 1.227$ kg/m^3 (0.00238 slugs/ft^3)

ambient sonic velocity, $c_a = c_{ISA} = 340$ m/sec (1116 ft/sec)

I. Calculate the OASPL at $\theta = 90^{o}$ for the core jet alone from equation (16) with core jet properties:

$$OASPL_{90^o} - 10 \log\left[\left(\frac{A_{j,1}}{R^2}\right)\left(\frac{\rho_a}{\rho_{ISA}}\right)^2\left(\frac{c_a}{c_{ISA}}\right)^4\right]$$

$$- 10\left\{\frac{3\left[\left(\frac{V_{j,1}}{c_a}\right)\left(1 - \frac{V_a}{V_{j,1}}\right)^{3/4}\right]^{3.5}}{0.60 + \left[\left(\frac{V_{j,1}}{c_a}\right)\left(1 - \frac{V_a}{V_{j,1}}\right)^{3/4}\right]^{3.5}} - 1\right\}\log\left(\frac{\rho_{j,1}}{\rho_a}\right) = 141$$

$$+ 10 \log\left\{\frac{\left[\left(\frac{V_{j,1}}{c_a}\right)\left(1 - \frac{V_a}{V_{j,1}}\right)^{3/4}\right]^{7.5}}{1 + 0.010\left[\left(\frac{V_{j,1}}{c_a}\right)\left(1 - \frac{V_a}{V_{j,1}}\right)^{3/4}\right]^{4.5}}\right\}$$

$$+ 3 \log\left(0.10 + 2\frac{h_1}{D_1}\right)$$

Substituting the given values:

$$\text{(a)}\ \log\left[\left(\frac{A_{j,1}}{R^2}\right)\left(\frac{\rho_a}{\rho_{ISA}}\right)^2\left(\frac{c_a}{c_{ISA}}\right)^4\right] = \log\left(\frac{A_{j,1}}{R^2}\right) = \log\left(\frac{3}{10^4}\right) = -3.52$$

(b) $$\log\left(0.10 + 2\frac{h_1}{D_1}\right) = \log\left(0.10 + 2\frac{0.49}{2.44}\right) = -0.301$$

$$\frac{V_{j,1}}{c_a} = \frac{1200}{1116} = 1.075; \quad \left(1 - \frac{V_a}{V_j}\right)^{3/4} = \left(1 - \frac{400}{1200}\right)^{3/4} = 0.738$$

$$\left(\frac{V_{j,1}}{c_a}\right)\left(1 - \frac{V_a}{V_{j,1}}\right)^{3/4} = (1.075)(0.738) = 0.793$$

(c) $$\left\{\frac{3\left[\left(\frac{V_{j,1}}{c_a}\right)\left(1 - \frac{V_a}{V_{j,1}}\right)^{3/4}\right]^{3.5}}{0.60 + \left[\left(\frac{V_{j,1}}{c_a}\right)\left(1 - \frac{V_a}{V_{j,1}}\right)^{3/4}\right]^{3.5}} - 1\right\}\log\left(\frac{\rho_{j,1}}{\rho_a}\right)$$

$$= \left\{\frac{3(0.793)^{3.5}}{0.60 + (0.793)^{3.5}} - 1\right\}\log\left(\frac{0.00109}{0.00238}\right) = 0.276\log(0.462) = -0.0914$$

(d) $$\log\left\{\frac{\left[\left(\frac{V_{j,1}}{c_a}\right)\left(1 - \frac{V_a}{V_{j,1}}\right)^{3/4}\right]^{7.5}}{1 + 0.010\left[\left(\frac{V_{j,1}}{c_a}\right)\left(1 - \frac{V_a}{V_{j,1}}\right)^{3/4}\right]^{4.5}}\right\} = \log\left[\frac{(0.793)^{7.5}}{1 + 0.0010(0.793)^{4.5}}\right] = -0.758$$

(e) $OASPL_{90^o,1} = 141 + 10(-3.52) + 10(-0.0914) + 3(-0.301) + 10(-0.758)$

$= 96.4$

II. Calculate the OASPL at $\theta = 90^o$ for the coaxial jets, by computing the increase or decrease from the core jet alone from equation (18):

$$OASPL_{90^o} - OASPL_{90^o,1} = 5 \log \left(\frac{T_{j,1}}{T_{j,2}}\right) + 10 \log \left[\left(1 - \frac{V_{j,2}}{V_{j,1}}\right)^m + 1.2 \frac{\left(1 + \frac{A_{j,2} V_{j,2}^2}{A_{j,1} V_{j,1}^2}\right)^4}{\left(1 + \frac{A_{j,2}}{A_{j,1}}\right)^3} \right]$$

(a) $5 \log \left(\frac{T_{j,1}}{T_{j,2}}\right) = 10 \log \left(\frac{1260}{580}\right)^{1/2} = 1.68$

$\frac{V_{j,2}}{V_{j,1}} = \frac{960}{1200} = 0.800; \quad \frac{A_{j,2}}{A_{j,1}} = 3.40$

$m = 1.1 \sqrt{\frac{A_{j,2}}{A_{j,1}}} = 1.1 \sqrt{3.4} = 2.03$

$\left(1 - \frac{V_{j,2}}{V_{j,1}}\right)^m = (1 - 0.800)^{2.03} = 0.0381$

$$\frac{1.2}{\left(1+\frac{A_{j,2}}{A_{j,1}}\right)^3}\left[1+\left(\frac{A_{j,2}}{A_{j,1}}\right)\left(\frac{V_{j,2}}{V_{j,1}}\right)^2\right]^4 = \frac{1.2}{(1+3.40)^3}\left[1+3.40(0.800)^2\right]^4 = 1.434$$

(b) $$10 \log \left[\left(1-\frac{V_{j,2}}{V_{j,1}}\right)^m + 1.2\,\frac{\left(1+\frac{A_{j,2}V_{j,2}^2}{A_{j,1}V_{j,1}^2}\right)^4}{\left(1+\frac{A_{j,2}}{A_{j,1}}\right)}\right] = 10 \log (1.472) = 1.67$$

(c) $OASPL_{90^o} - OASPL_{90^o,1} = 1.68 + 1.67 = 3.35$

(d) $OASPL_{90^o} = 96.4 + 3.35 = 99.7$

III. Determine the frequency-shift parameter $\left[1-(S_1/S)\right]\left[(T_{j,1})/(T_{j,2})\right]$ from figure 12, and thus the Strouhal number ratio S/S_1:

(a) Abscissa, $\log\left[1+(A_{j,2})/(A_{j,1})\right] = \log(1+3.40) = 0.643$.

(b) For $V_{j,2}/V_{j,1} = 0.8$, the value of the frequency-shift parameter is 0.515.

(c) $1-(S_1)/(S) = 0.515\left[(T_{j,2})/(T_{j,1})\right] = 0.515\left[(580)/(1260)\right] = 0.237$

$S_1/S = 0.763$, so $S/S_1 = 1.311$

IV. Determine the SPL spectrum for $\theta = 150^o$ from figure 5.

(a) Calculate the convection Mach number from equation (4):

$$M_c = 0.62 \left(\frac{V_j - V_o}{c_a} \right) = \left(\frac{1200 - 400}{1116} \right) = 0.444$$

(b) Calculate the convective directivity factor:

$$30 \log \left(1 + \frac{M_c}{\sqrt[5]{1 + M_c^5}} \cos \theta \right) = 30 \log \left(1 + \frac{0.444}{\sqrt[5]{1 + (0.444)^5}} \cos \theta \right)$$

$$= 30 \log \left[1 + 0.443(-0.866) \right]$$

$$= -6.30 \text{ dB}$$

(c) Determine the effective angle:

$$\theta' = \theta \left(\frac{V_j}{c_a} \right)^{0.1} = 150(1.075)^{0.1} = 151$$

(d) Compute the ratio of Strouhal number S to center frequency:

$$S = \left(\frac{S}{S_1} \right) \left(\frac{D_{e,1}}{V_{j,1}} \right) \left(\frac{D_{h,1}}{D_{e,1}} \right)^{0.4} \left(\frac{T_{j,1}}{T_{ISA}} \right)^{0.4(1+\cos\theta')} f$$

where

$$D_{e,1} = \sqrt{\frac{4}{\pi} A_{j,1}} = \sqrt{\frac{4(3)}{\pi}} = 1.95 \text{ ft}$$

and

$$D_{h,1} = 2h = 2(0.49) = 0.98 \text{ ft}$$

$$\frac{S}{f} = 1.311\left(\frac{1.95}{1200}\right)\left(\frac{0.98}{1.95}\right)^{0.4}\left(\frac{1260}{519}\right)^{0.4(1+\cos 151^{o})}$$

$$= 1.311\left(\frac{1.95}{1200}\right)(0.759)(2.43)^{0.0492} = 1.69\times10^{-3}$$

(e) For each center frequency f, compute log S and determine the ordinate, $\text{SPL-OASPL}_{90^{o}} + 30 \log \left(1 + \frac{M_c}{\sqrt[5]{1 + M_c^5}} \cos\theta\right)$, from figure 5, interpolating to $\theta' = 151$; then determine the SPL:

Nominal center frequency, f, Hz	log S	Ordinate $SPL - OASPL_{90^o} + 30 \log \left(1 + \frac{M_c \cos \theta}{\sqrt[5]{1 + M_c^5}}\right)$ at $\theta' = 151^o$	Free-field SPL, ordinate +106.0
31.5	-1.27	-20.7	85.3
40	-1.17	-17.5	88.5
50	-1.07	-15.0	91.0
63	-.97	-12.7	93.3
80	-.87	-11.0	95.0
100	-.77	-9.7	96.3
125	-.67	-8.9	97.1
160	-.57	-8.4	97.6
200	-.47	-8.9	97.1
250	-.37	-10.2	95.8
315	-.27	-11.6	94.4
400	-.17	-13.2	93.8
500	-.07	-14.8	91.2
630	.03	-16.5	89.5
800	.13	-18.2	87.8
1 000	.23	-19.8	86.2
1 250	.33	-21.5	84.5
1 600	.43	-23.2	82.8
2 000	.53	-24.9	81.1
2 500	.63	-26.6	79.4
3 150	.73	-28.3	77.7
4 000	.83	-30.0	76.0
5 000	.93	-31.7	74.3
6 300	1.03	-33.4	72.6
8 000	1.13	-35.1	70.9
10 000	1.23	-36.7	69.3
12 500	1.33	-38.4	67.6
16 000	1.43	-40.1	65.9
20 000	1.53	-41.7	64.3

REFERENCES

1. Lighthill, M. J.: On Sound Generated Aerodynamically. I. General Theory. Proc. Roy. Soc. (London), ser. A, vol. 211, No. 1107, Mar. 1952, pp. 564-587.

2. Lighthill, M. J.: On Sound Generated Aerodynamically. II. Turbulence as a Source of Sound. Proc. Roy. Soc. (London), ser. A, vol. 222, No. 1148, Feb. 1954, pp. 1-32.

3. Sanders, N. D.; and Lawrence, J. C.: Fundamental Investigation of Noise Generation by Turbulent Jets. SAE Trans., vol. 65, 1957, pp. 244-249.

4. Knott, P. R.; and Benzakein, M. J.: Analytical and Experimental Supersonic Jet Noise Research. AIAA Paper 73-188, Jan. 1973.

5. Wooldridge, C. E.; Wooten, D. C.; and Amaro, A. J.: The Structure of Jet Turbulence Producing Jet Noise. AIAA Paper 72-158, Jan. 1972.

6. Ribner, Herbert S.: On the Strength Distribution of Noise Sources Along a Jet. UTIA Rept. 51, University of Toronto, 1958.

7. Lilley, G. M.: On the Noise of Air Jets. ARC 20,376, Aeronautical Research Council, 1958.

8. Pao, S. P.; and Lowson, M. V.: Some Applications of Jet Noise Theory. AIAA Paper 70-233, Jan. 1970.

9. Rotta, J. C.: Berechnung der Abgestrahlten Schallenergie Turbulenter Stromungen (Computation of the Sound Energy Radiated from Turbulent Flows). Presented at Deutsche Gesellschaft fur Luft- und Raumfahrt, Jahrestagung, 5th, Berlin, West Germany, Oct. 4-6, 1972, Paper 72-074.

10. Chu, Wing T.: Turbulence Measurements Relevant to Jet Noise. UTIAS 119, Univ. of Toronto (AD-645322), 1966.

11. Wilson, L. N.; Krause, F. R.; and Kadrmas, K. A.: Optical Measurements of Sound Source Intensities in Jets. Basic Aerodynamic Noise Research. NASA SP 207, 1969, pp. 147-160.

12. Damkevalva, R. J.; Grosche, F. R.; and Guest, F.: Sound Source Measurement in Model Air Jets Using the Crossed-Beam Correlation Technique. Paper presented at AGARD Specialists Meeting on Noise Mechanisms, Brussels, Belgium, Sept. 1973.

13. Ffowcs Williams, J. E.: Some Thoughts on the Effects of Aircraft Motion and Eddy Convection on the Noise from Air Jet. USAA Rept. 155, Southhampton Univ. (Gt. Britain), 1960.

14. Ribner, H. S.: The Generation of Sound by Turbulence Jets. Advances in Applied Mechanics, Vol. 8, Academic Press, 1964, pp. 103-182.

15. Goldstein, Marvin E.; and Howes, Walton L.: New Aspects of Subsonic Aerodynamic Noise Theory. NASA TN D-7158, 1973.

16. Ribner, H. S.: Quadrupole Correlations Governing the Pattern of Jet Noise. J. Fluid Mech., vol. 38, part I, Aug. 14, 1969, pp. 1-24.

17. Olsen, W. A.; Gutierrez, O. A.; and Dorsch, R. G.: The Effect of Nozzle Inlet Shape, Lip Thickness, and Exit Shape and Size on Subsonic Jet Noise. AIAA Paper 73-187, Jan. 1973.

18. Lush, P. A.: Measurements of Subsonic Jet Noise and Comparison with Theory. J. Fluid Mech., vol. 46, pt. 3, Apr. 13, 1971, pp. 477-500.

19. Krishnappa, G.; and Csanady, G. T.: An Experimental Investigation of the Composition of Jet Noise. J. Fluid Mech., vol. 37, pt. 1, June 5, 1969, pp. 149-159.

20. Howes, Walton L.: Similarity of Far Noise Fields of Jets. NASA TR R-52, 1960.

21. Cowan, S. J.; and Crouch, R. W.: Transmission of Sound Through a Two-Dimensional Shielding Jet. AIAA Paper 73-1002, Oct. 1973.

22. Miles, John W.: On the Reflection of Sound at an Interface of Relative Motion. J. Acoust. Soc. Am., vol. 29, no. 2, Feb. 1951, pp. 226-228.

23. Ribner, Herbert S.: Reflection, Transmission, and Amplification of Sound Waves by a Moving Medium. J. Acoust. Soc. Am., vol. 29, no. 4, Apr. 1957, pp. 435-441.

24. Yeh, C.: A Further Note on the Reflection and Transmission of Sound Waves by a Moving Fluid Layer. J. Acoust. Soc. Am., vol. 43, no. 6, June 1968, pp. 1454-1455.

25. Graham, E. W.; and Graham, B. B.: Effect of a Shear Layer on Plane Waves of Sound in a Fluid. J. Acoust. Soc. Am., vol. 46, no. 1, 1969, pp. 169-175.

26. Rudnick, I.: Acoustic Transmission Through a Fluid Lamina. J. Acoust. Soc. Am., vol. 17, no. 3, Jan. 1946, pp. 245-253.

27. Jones, Ian S. F.: Jet Noise Suppression by an Impedance Shroud. D1-82-0984, Boeing Scientific Research Labs. (AD-712406), 1970.

28. Norum, Thomas D.: Measured and Calculated Transmission Losses of Sound Waves Through a Helium Layer. NASA TN D-7230, 1973.

29. Atvars, J.; Schubert, L. K.; and Ribner, H. S.: Refraction of Sound from a Point Source Placed in an Air Jet. AIAA Paper 65-82, Jan. 1965.

30. Atvars, J.; Schubert, L. K.; Grande, E.; and Ribner, H. S.: Refraction of Sound by Jet Flow or Jet Temperature. NASA CR-494, 1966.

31. Grande, E.: Refraction of Sound by Jet Flow and Jet Temperature. Extension of Temperature Range Parameters and Development of Theory. NASA CR-840, 1967.

32. McGregor, G. R.; Ribner, H. S.; and Lam, H.: "Basic" Jet Noise Patterns after Deletion of Convection and Refraction Effects: Experiments vs. Theory. J. Sound Vibration, vol. 27, no. 4, Apr. 22, 1973, pp. 437-454.

33. deBelleval, J. F.; Random, J.; Perulli, M.; and Taillefesse, J. C.: Influence of Refraction Effects on the Interpretation of Hot Jet Noise. AIAA Paper 73-990, Oct. 1973.

34. Csanady, G. T.: The Effect of Mean Velocity Variations on Jet Noise. J. Fluid Mech., vol. 26, pt. 1, Sept, 1966, pp. 183-197.

35. Ahuja, K. K.: Correlation and Prediction of Jet Noise. J. Sound Vibration, vol. 29, no. 2, July 22, 1973, pp. 155-168.

36. Olsen, W. A.; and Friedman, R.: Jet Noise From Coaxial Nozzles Over a Wide Range of Geometric and Flow Parameters. AIAA Paper No. 74-43, Jan. 1974.

37. Bushell, K. W.: A Survey of Low Velocity and Coaxial Jet Noise with Application to Prediction. J. Sound Vibration, vol. 17, no. 2, July 22, 1971, pp. 271-282.

38. Dunn, D. G.; and Peart, N. A.: Aircraft Noise Source and Contour Estimation. (D6-60233, Boeing Commercial Airplane Co.) NASA CR-114649, 1973.

39. Jet Noise Prediction. Aerospace Information Rept. 876, SAE, July 10, 1965.

40. Anon.: Standard Values of Atmospheric Absorption as a Function of Temperature and Humidity for Use in Evaluating Aircraft Flyover Noise. Aerospace Recommended Practice 866, SAE, Aug. 1964.

41. von Glah, U. H.: Correlation of Total Sound Power and Peak Sideline OASPL from Jet Exhausts. AIAA Paper 72-643, June 1972.

42. Simcox, C. D.: Effect of Temperature and Shock Structure on Choked Jet Noise Characteristics. AIAA Paper 71-582, June 1971.

43. Callaghan, E. E.; and Coles, W. D. Far Noise Field of Air Jets and Jet Engines. NACA TR-1329, 1957.

44. Dorsch, R. G.; Kreim, W. J.; and Olsen, W. A.: Externally Blown-Flap Noise. AIAA Paper 72-129, Jan. 1972.

45. Olsen, William A.; Dorsch, Robert G., and Miles, Jeffrey H.: Noise Produced by a Small-Scale Externally Blown Flap. NASA TN D-6636, 1972.

46. Minner, G. L.; and Feiler, C. E.: Low-Speed Jet Noise from a 1.83-Meter (6-Ft) Fan for Turbofan Engines. AIAA Paper 71-586, June 1971.

47. Plumblee, H. E.; Wynne, G. A.; and Zinn, B. T.: Effects of Jet Temperature on Jet and Pure Tone Noise Radiation. NASA CR-1472, 1969.

48. Hoch, R. G.; Duponchel, J. P.; Cocking, B. J.; and Bryce, W. D.: Studies of the Influence of Jet Density on Jet Noise. Presented at First International Symposium on Air Breathing Engines, Marseille, France, June 19-23, 1972.

49. Swan, Walter C.; and Simcox, Craig D.: A Status Report on Jet Noise Suppression as Seen by an Aircraft Manufacturer. AIAA Paper 73-816, Aug. 1973.

50. Tanna, H. K.; Fisher, M. J.; and Dean, P. D.: Effect of Temperature on Supersonic Jet Noise. AIAA Paper 73-991, Oct. 1973.

51. Morfey, C. L.: Amplification of Aerodynamic Noise by Convected Flow Inhomogeneities. J. Sound Vibration, vol. 31, no. 4, Dec. 8, 1973, pp. 391-397.

52. Burrin, R. H.; Dean, P. D.; and Tanna, H. K.: A New Anechoic Facility for Supersonic Hot Jet Noise Research at Lockheed-Georgia. Presented at 86th Meeting of the Acoustical Society of America, Los Angeles, Calif., Oct. 30 - Nov. 2, 1973, Paper H9.

53. Karchmer, Allen M., Dorsch, Robert G.; and Friedman, Robert: Acoustic Tests of a 15.2-cm Diameter Potential Flow Nozzle. NASA TM X-2980, 1974.

54. von Glahn, Uwe H.; Gray, Vernon H.; Krejsa, Eugene A.; Lee, Robert; and Minner, Gene L.: Jet Noise. Aircraft Engine Noise Reduction. NASA SP-311, 1972, pp. 103-138.

55. Atvars, J.; Paynter, G. C.; Walker, D. Q.; and Wintermeyer, C. F.: Development of Acoustically-Lined Ejector Technology for Multilube Jet Noise Suppresser Nozzles by Model Engine Tests Over a Wide Range of Jet Pressure Ratios and Temperatures. NASA CR-2382, 1974.

56. Rollin, V. G.: Effect of Jet Temperature on Jet Noise Generation. NACA TN-4217, 1958.

57. Lassiter, L. W.; and Hubbard, H. H.: Experimental Studies of Noise from Subsonic Jets in Still Air. NACA TN-2757, 1952.

58. Mollo-Christensen, Erik; Kolpin, Marc A.; and Martucelli, John R.: Experiments on Jet Flow and Jet Noise Far Field Spectra and Directivity Patterns. ASRL-TR-1007, Massachusetts Inst. of Tech., 1963.

59. Lush, Peter A.; and Burrin, Robert H.: The Generation and Radiation of Supersonic Jet Noise. Volume 5: An Experimental Investigation of Jet Noise Variation with Velocity and Temperature. Lockheed Georgia Co. (AD-749140; AFAPL-TR-72-53-Vol. 5), 1972.

60. Nagamatsu, H. T.; Sheer, R. E., Jr.; and Horvay, G.: Supersonic Jet Noise Theory and Experiments. Basic Aerodynamic Noise Research. NASA SP-207, 1969, pp. 17-51.

61. Ribner, H. S.: Eddy-Mach Wave Noise From a Simplified Model of a Supersonic Mixing Layer. Basic Aerodynamic Noise Research. NASA SP-207, 1969, pp. 53-61.

62. Burley, Richard R., Karabinus, Raymond J.; and Freedman, Robert J.: Flight Investigation of Acoustic and Thrust Characteristics of Several Exhaust Nozzles Installed on Underwing Nacelles on an F106 Airplane. NASA TM X-2854, 1973.

63. Burley, Richard R.; and Karabinus, Raymond J.: Flyover and Static Tests to Investigate External Flow Effect on Jet Noise for Non-Suppressor and Suppressor Exhaust Nozzles. AIAA Paper 73-190, Jan. 1973.

64. Brausch, J. F.: Flight Velocity Influence on Jet Noise of Conical Ejector, Annular Plug and Segmented Suppressor Nozzles. (General Electric Co.; Contract NAS3-15773) NASA CR-120961, 1972.

65. Coles, Willard D.; Mihaloew, John A.; and Swann, William H.: Ground and In-Flight Acoustic and Performance Characteristics of Jet-Aircraft Exhaust Noise Suppressors. NASA TN D-874, 1961.

66. Ffowcs Williams, J. E.: The Noise From Turbulence Convected at High Speed. Phil. Trans. Roy. Soc., London, ser. A, vol. 255, no. 1061, Apr. 18, 1963, pp. 469-503.

67. von Glahn U.; Groesbeck, D.; and Goodykoontz, J.: Velocity Decay and Acoustic Characteristics of Various Nozzle Geometries with Forward Velocity. AIAA Paper 73-629, July 1973.

68. Stone, James R., and Gutierrez, Orlando A.: Small-Scale Noise Tests of a Slot Nozzle with V-Gutter Target Thrust Reverser. NASA TM X-2758, 1973.

69. Reshotko, Meyer; Olsen, William A.; and Dorsch, Robert G.: Preliminary Noise Tests of the Engine-Over-the-Wing Concept. I: 30 Deg - 60 Deg Flap Position. NASA TM X-68032, 1972.

70. Stone, J. R.; and Gutierrez, O. A.: Noise Tests of a High-Aspect-Ratio Slot Nozzle with Various V-Gutter Target Thrust Reversers. Presented At 86th Meeting of the Acoustical Society of America, Los Angeles, Calif., Oct. 30-Nov. 2, 1973, paper Z8.

71. Design Integration and Noise Study for a Large STOL Augmentor Wing Transport. D6-60139. Boeing Co., 1971.

72. Grosche, F. R.: Measurements of the Noise of Air Jets from Slot Nozzles With and Without Shields. AVA-FB-6802, Aerodynamische Versuchsanstalt (West Germany) (DLR-FB-68-46), 1968.

73. Coles, Willard D.: Jet Engine Exhaust Noise from Slot Nozzles. NASA TN D-60, 1959.

74. Williams, T. J.; Ali, M. R. M. H.; and Anderson, J. S.: Noise and Flow Characteristics of Coaxial Jets. J. Mech. Eng. Sci., vol. 11, no. 2, Apr. 1969, pp. 133-142.

75. Eldred, Kenneth M.: Far Field Noise Generation by Coaxial Flow Jet Exhausts. Volume I: Detailed Description. Wyle Labs., Inc. (FAA-RD-71-101-Vol. 1), 1971.

76. Dosanjh, Darshan S.; Abdelhamid, Amr N.; and Yu, James C.: Noise Reduction From Interacting Coaxial Supersonic Jet Flows. Basic Aerodynamic Noise Research. NASA SP-207, 1969, pp. 63-101.

77. Yu, J. C.; and Dosanjh, D. S.: Noise Field of Interacting Supersonic Jet Flows. AIAA Paper 71-152, Jan. 1971.

78. Dosanjh, Darshan S.; Yu, James C.; Abdelhamid, Amr N.: Reduction of Noise from Supersonic Jet Flows. AIAA J., vol. 9, no. 12, Dec. 1971, pp. 2346-2353.

79. Gray, Vernon H.; Gutierrez, Orlando A.; and Walker, David Q.: Assessment of Jets as Acoustic Shields by Comparison of Single- and Multitube Suppressor Nozzle Data. AIAA Paper 73-1001, Oct. 1973.

80. Greatrex, F. B.: Noise Suppressors for Avon and Conway Engines. ASME Paper 59-AV-49, Mar. 1959.

81. Eldred, Kenneth E.; White, Robert W.; Mann, Myron A.; and Cottis, Miltiades G.: Suppression of Jet Noise with Emphasis on the Near Field. ASD-TDR-62-578, Wright-Patterson AFB, 1963.

82. Nagamatsu, H. T.; Sheer, R. E., Jr.; and Bigelow, E. C.: Subsonic and Supersonic Jet Flow and Acoustic Characteristics and Supersonic Suppressors. (Rept. 72, General Electric Co., Contract NASw-1784) NASA CR-125594, 1972.

83. Middleton, Derek; and Clark, Patrick J. F.: Assessment and Development of Methods of Acoustic Performance Prediction for Jet Noise Suppressors. UTIAS-TN-134, University of Toronto (AFOSR 69-0780TR; AD-687475), 1969.

84. Ciepluch, C. C.; North, W. J.; Coles, W. D.; and Antl, R. J.: Acoustic, Thrust, and Drag Characteristics of Several Full-Scale Noise Suppressors for Turbojet Engines. NACA TN-4261, 1958.

85. Nagamatsu, H. T.; and Sheer, R. E., Jr.: Flow, Thrust, and Acoustic Characteristics of 50 Tubes with 50 Shrouds Supersonic Jet Noise Suppressor. AIAA Paper 72-642, June 1972.

86. Schairer, G. S., O'Keefe, J. V.; and Johnson, P. E.: Perspective of SST Aircraft Noise Problem, I: Acoustic Design Considerations. J. Aircraft, vol. 8, no. 1, Jan. 1971, pp. 19-25.

87. Huff, Ronald G.; and Groesbeck, Donald E.: Splitting Supersonic Nozzle Flow Into Separate Jets by Overexpansion Into a Multilobed Divergent Nozzle. NASA TN D-6667, 1972.

88. Jordan, L. R.; and Auble, C. M.: Development of the Suppressor and Thrust Brake for the DC-8 Airplane. SAE Paper 85A, Sept. 29-Oct. 4, 1958.

89. Goodykoontz, Jack H.; Dorsch, Robert G.; and Groesbeck, Donald E.: Noise Tests of a Mixer Nozzle-Externally Blown Flap System. NASA TN D-7236, 1973.

90. Jones, W. L.; and Heidelberg, L. J.: Investigation of Noise from Full-Scale High Bypass Engine and Blown Flap System. SAE Paper 740467, April-May 1974.

91. Gutierrez, Orlando A.; and Stone, James R.: Preliminary Experiments on Noise Generated by Target-Type Thrust Reverser Models. NASA TM X-2553, 1972.

92. Stone, J. R.; and Gutierrez, O. A.: Target-Type Thrust Reverser Noise. J. Aircraft, vol. 10, no. 5, May 1973, pp. 283-288.

93. Gutierrez, O. A.; Stone, J. R.; and Friedman, R.: Results from Cascade Thrust Reverser Noise and Suppression Experiments. AIAA Paper 74-36, Jan. 1974.

94. Fink, M. R.: Thrust Reverser Noise Estimation. J. Aircraft, vol. 10, no. 8, Aug. 1973, pp. 507-508.

95. Laurence, J. C.; and Bennighoff, J. M.: Turbulence Measurements in Multiple Interferring Air Jets. NACA TN-4029, 1957.

TABLE I. - SUMMARY OF RECOMMENDED INTERIM PREDICTION METHOD

Nozzle type	Method of predicting SPL (f, θ, and geometric, atmospheric, and jet variables)	
	Subsonic (and fully expanded supersonic)	Supersonic (not fully expanded)
Circular or slot	Figure 5 { $OASPL_{90^o}$ from eq. (12); M_c from eq. (14); S from eq. (17) }	*Figure 7 { OASPL (all θ) from eqs. (11) and (15); S from eq. (17) }
Plug	Figure 5 { $OASPL_{90^o}$ from eq. (16); M_c from eq. (14); S from eq. (17) }	*Figure 7 { OASPL (all θ) from eqs. (11) and (15); S from eq. (17) }
Coaxial	Figure 5 { $OASPL_{90^o}$ from eqs. (18) and (19) with core jet from eq. (12) or (16); M_c from eq. (14); S from eqs. (20) and (17) }	Core jet only supersonic: *Figure 7 { OASPL (all θ) from eqs. (11), (16), and (20); S from eqs. (22) and (23) } Bypass supersonic: Antilogarithmically add noise calculated treating bypass as a separate plug nozzle. and noise calculated for core jet alone
Target reversers	Figure 17 { $OASPL_{90^o}$ from eq. (21); $OASPL(\theta)$-$OASPL_{90^o}$ from eq. (22); S from eq. (17) }	Same as subsonic
Cascade reversers	Figure 19 { $OASPL_{90^o}$ from eqs. (23) to (25) and (6); $OASPL(\theta)$-$OASPL_{90^o}$ from eq. (26); S from eq. (17) }	Same as subsonic
Suppressors	Subsonic or supersonic: Antilogarithmically add premerging and postmerging noises (from ref. 38)	
	Premerging	Postmerging
(with shroud)	Eq. (B7) and figures 23 and 24 { $\overline{OASPL}$ from eqs. (B4) and (B5) with figures 21, 27, and 28; $OASPL(\theta)$-$\overline{OASPL}$ from eq. (B6) and figure 29 }	Eq. (B2) and figures 23 to 25 { $OASPL(\theta)$ from eq. (B1) and figures 21 and 22 }
(without shroud)	Same as above	Same as above with $\Delta OASPL(\theta)$ from eq. (B3) and figure 26 and with $V_{jm} = V_j$; $\rho_{jm} = \rho_j$; $T_{s,jm} = T_{s,j}$ and $D_{e,jm} = D_e\sqrt{R_A}$

*Add to subsonic jet noise antilogarithmically.

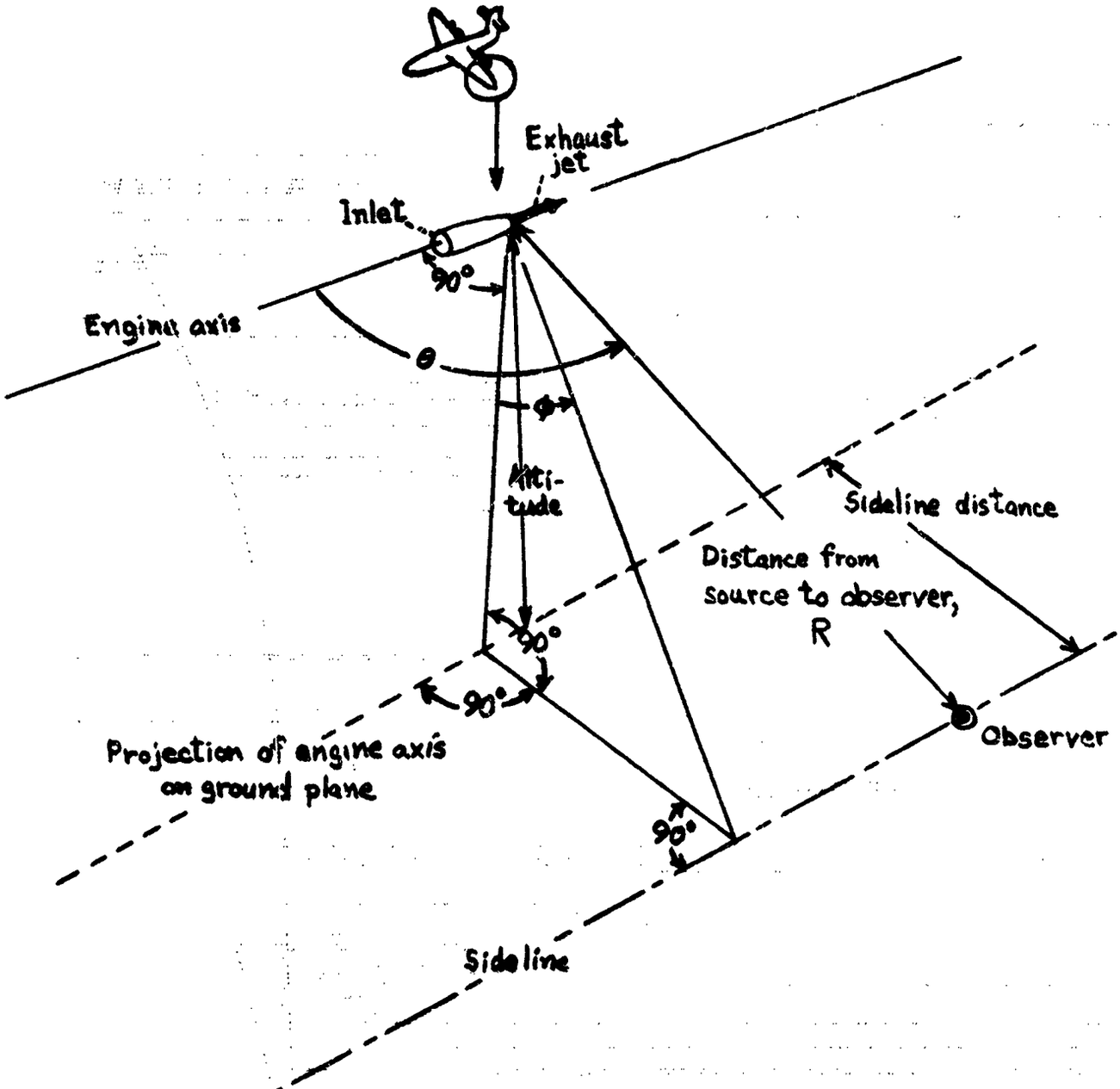

Figure 1. - Geometric variables describing position of airplane jet noise source with respect to an observation point.

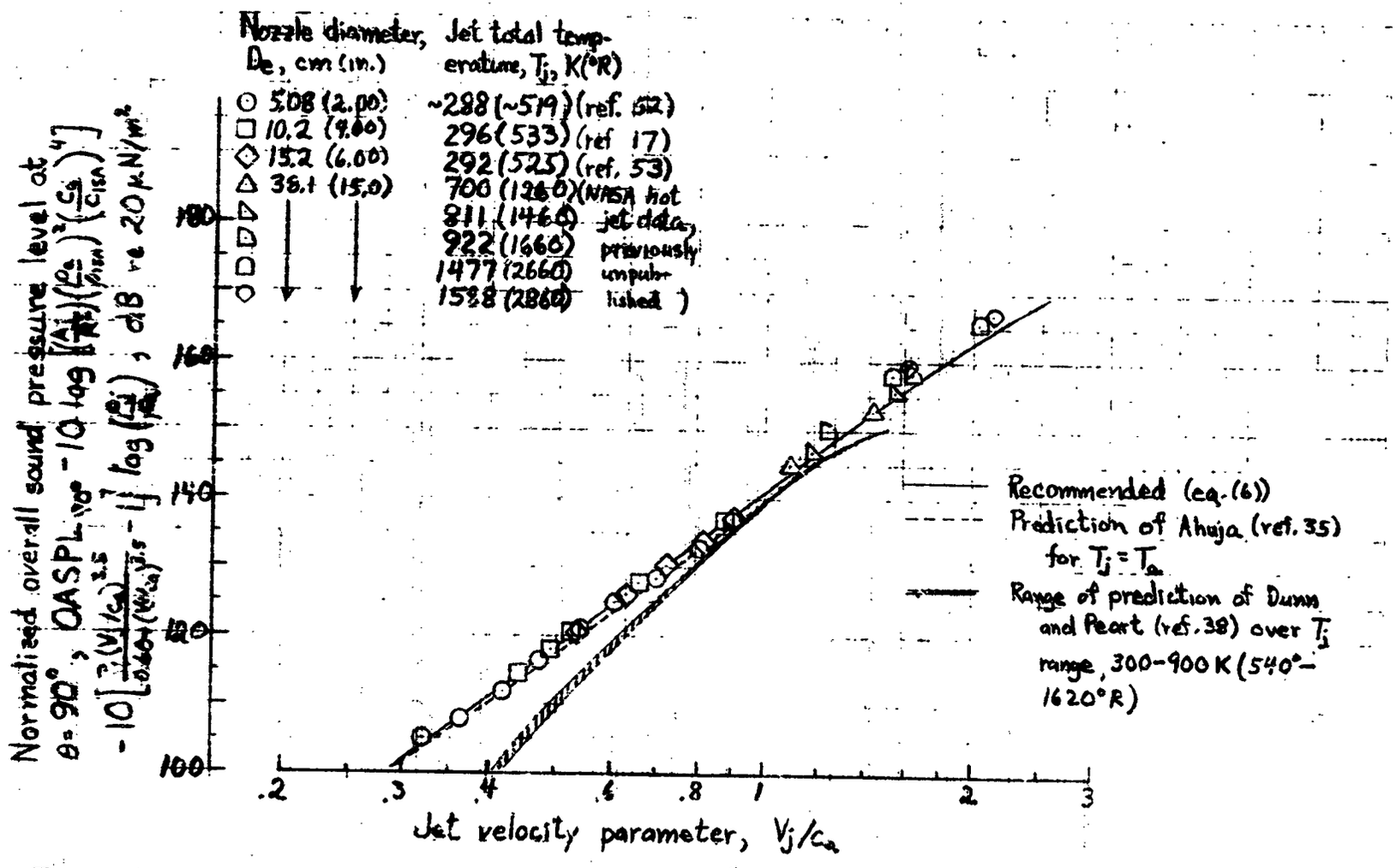

Figure 2.- Overall sound pressure level at θ = 90° for shock-free circular jets. Recommended prediction and comparison with experimental data and other predictions.

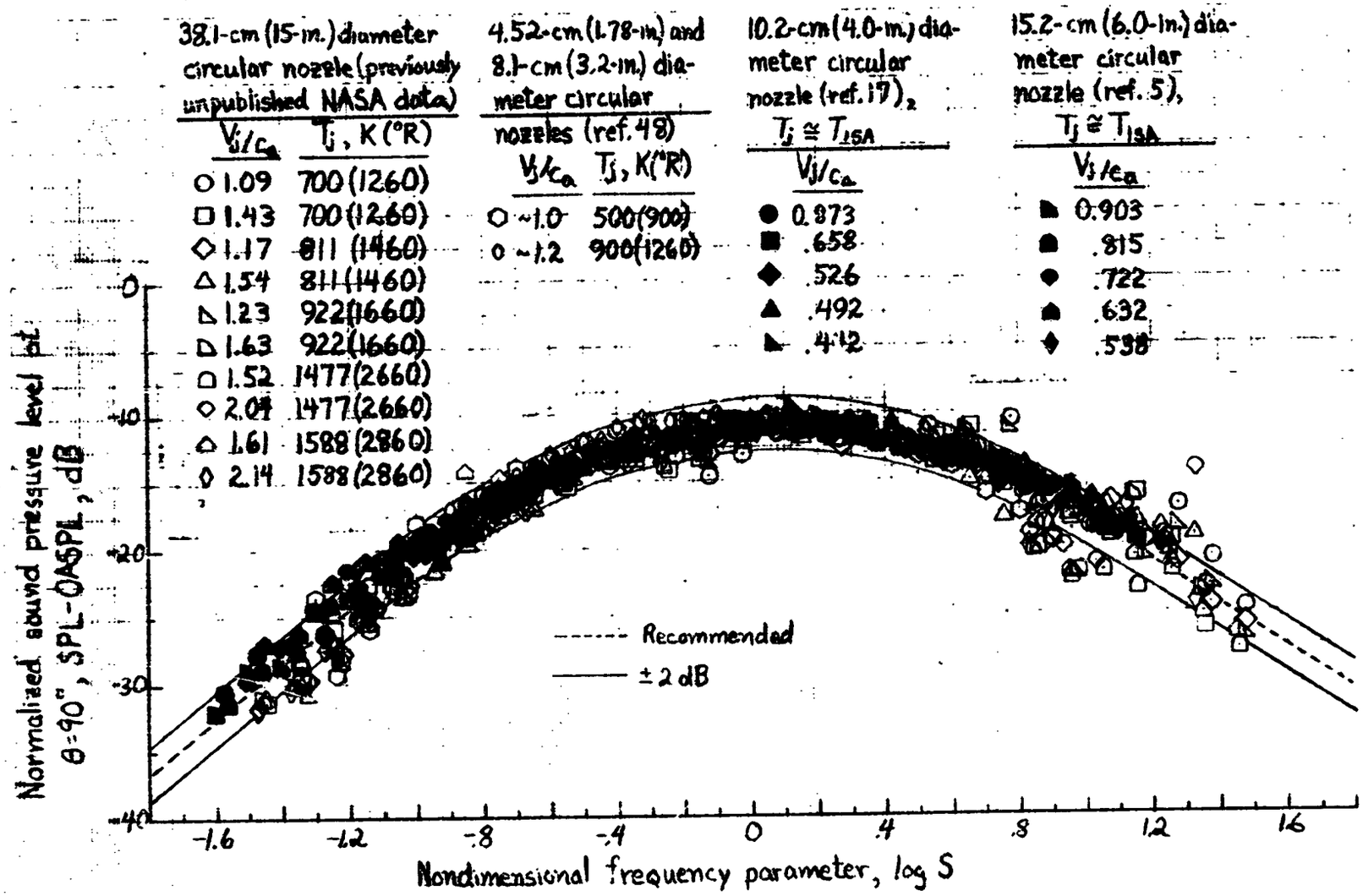

Figure 3.- Sound pressure level spectra at $\theta = 90°$ for shock-free circular jets; recommended relation and comparison with experimental data. (S defined in eq. (7).)

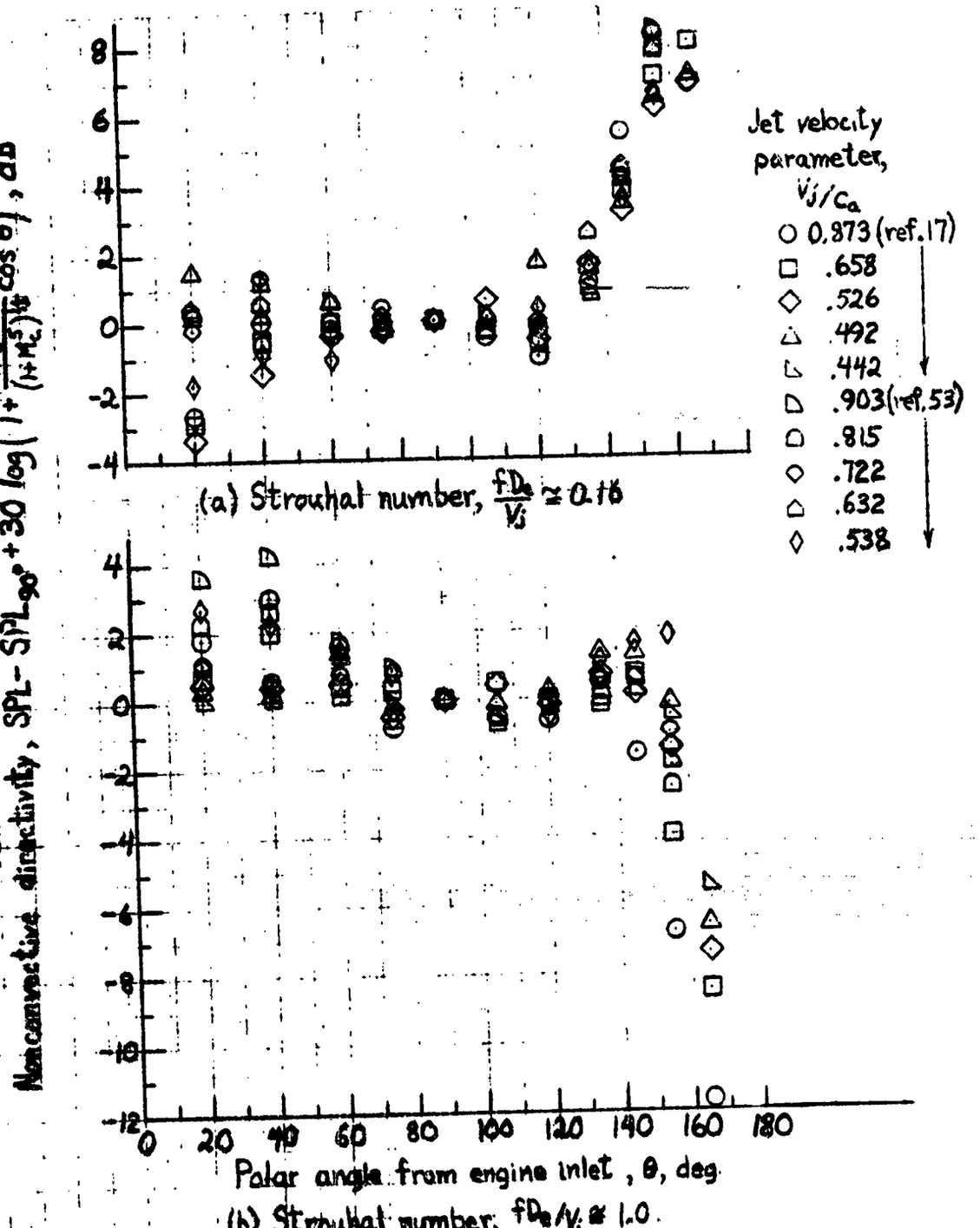

Figure 4.- 1/3-Octave-band jet noise directivity for ambient-temperature, shock-free circular jets.

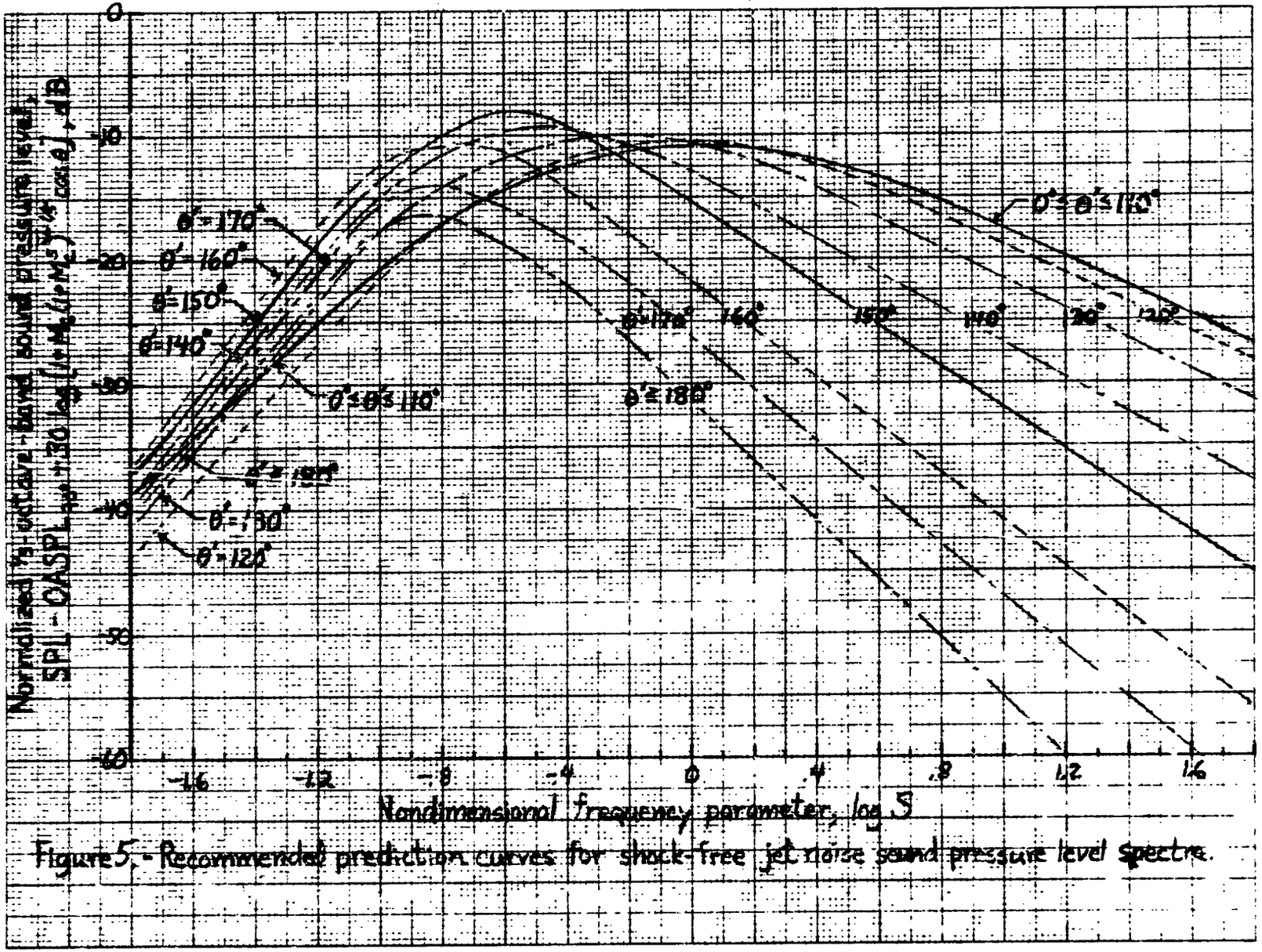

Figure 5. - Recommended prediction curves for shock-free jet noise sound pressure level spectra.

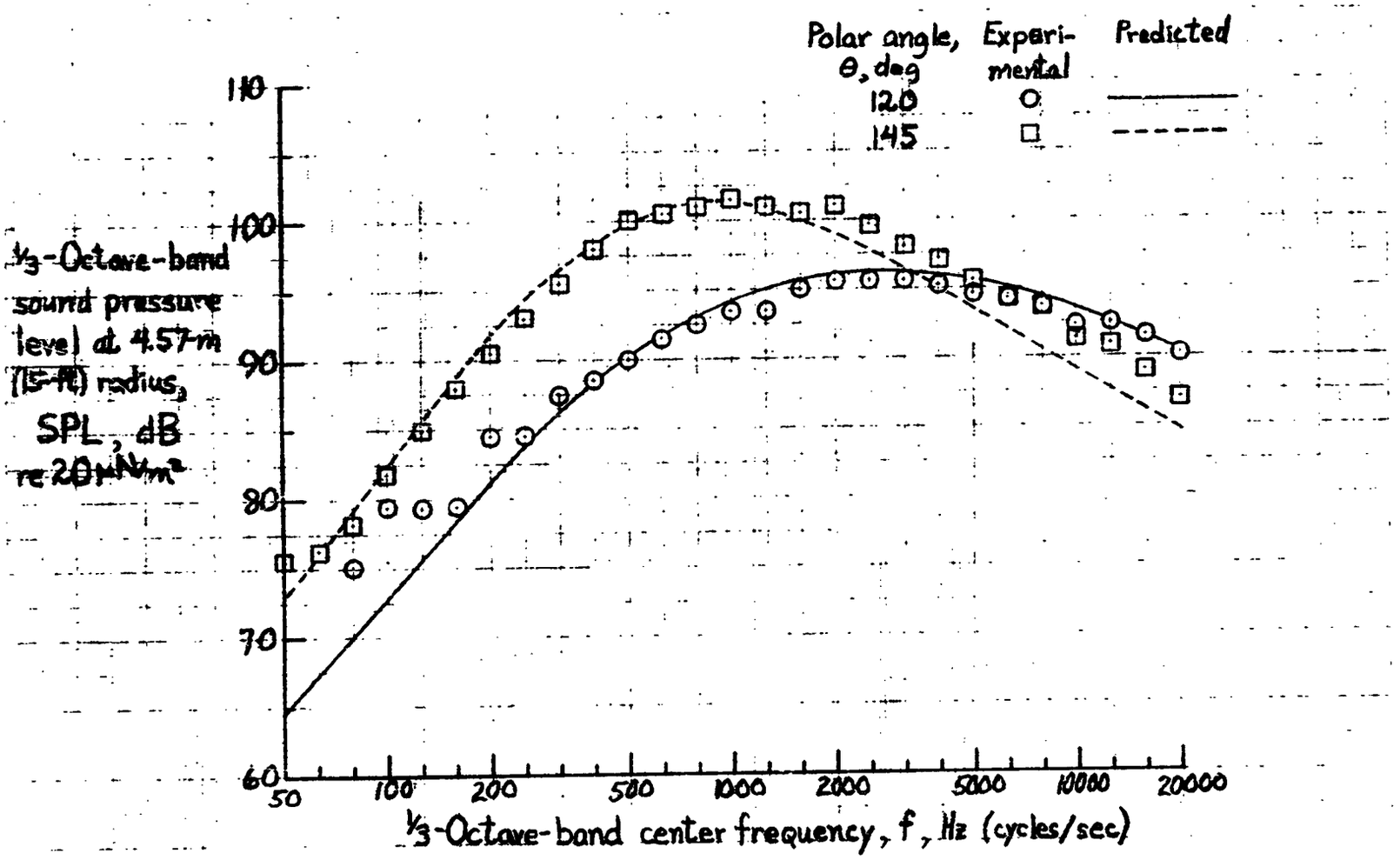

(a) 10.2-cm (4.0-in.) nozzle at approximately ambient total temperature and jet velocity, V_j = 302 m/sec (992 ft/sec).

Figure 6.- Comparison of experimental SPL spectra at various angles for shock-free circular nozzles with recommended prediction.

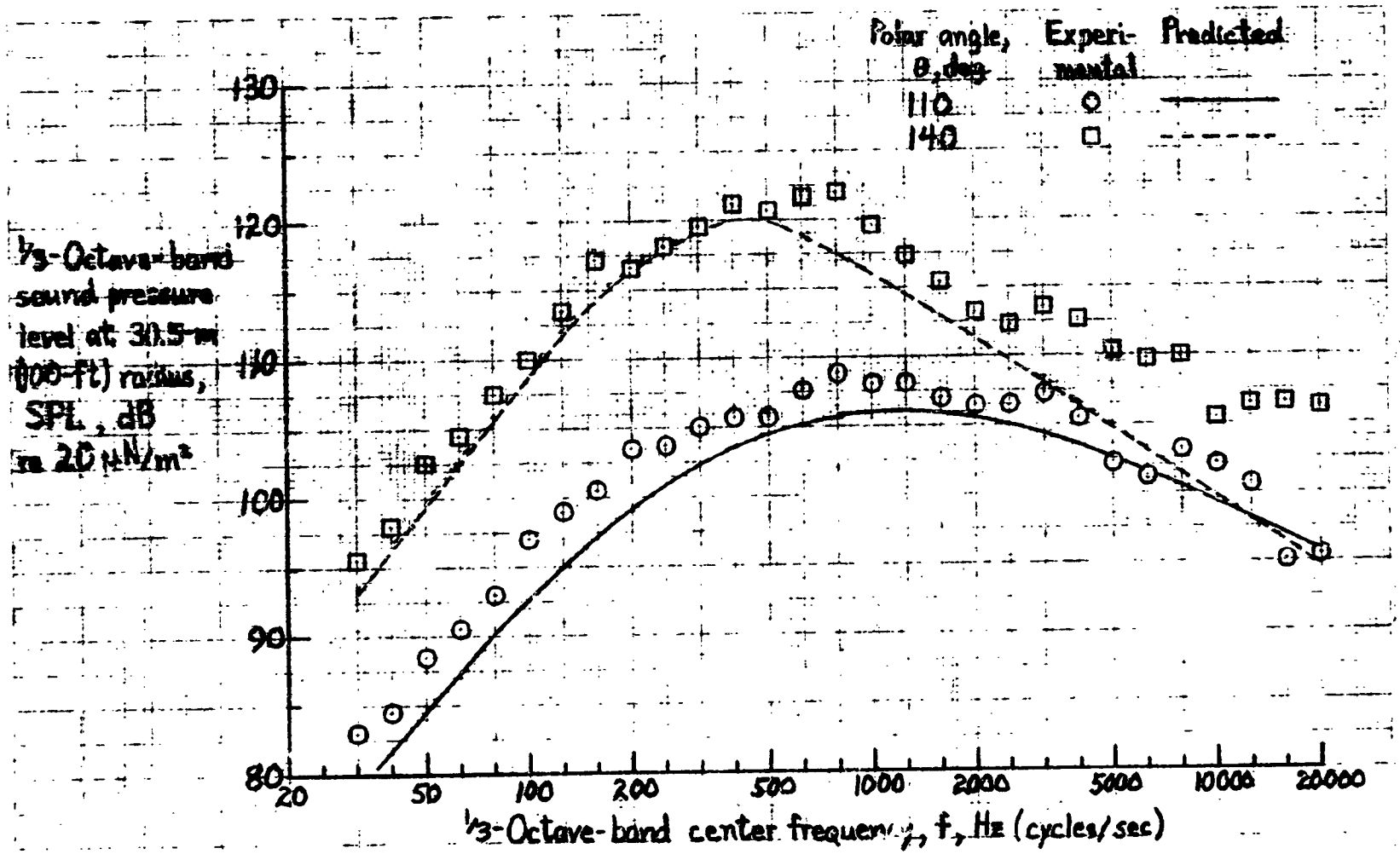

(b) 38.1-cm (15.0-in.) nozzle at jet total temperature, T_j = 1477 K (2660 °R), and jet velocity, V_j = 683 m/sec (2240 ft/sec)

Figure 6.- Concluded. Comparison of experimental SPL spectra at various angles for shock-free circular nozzles with recommended prediction.

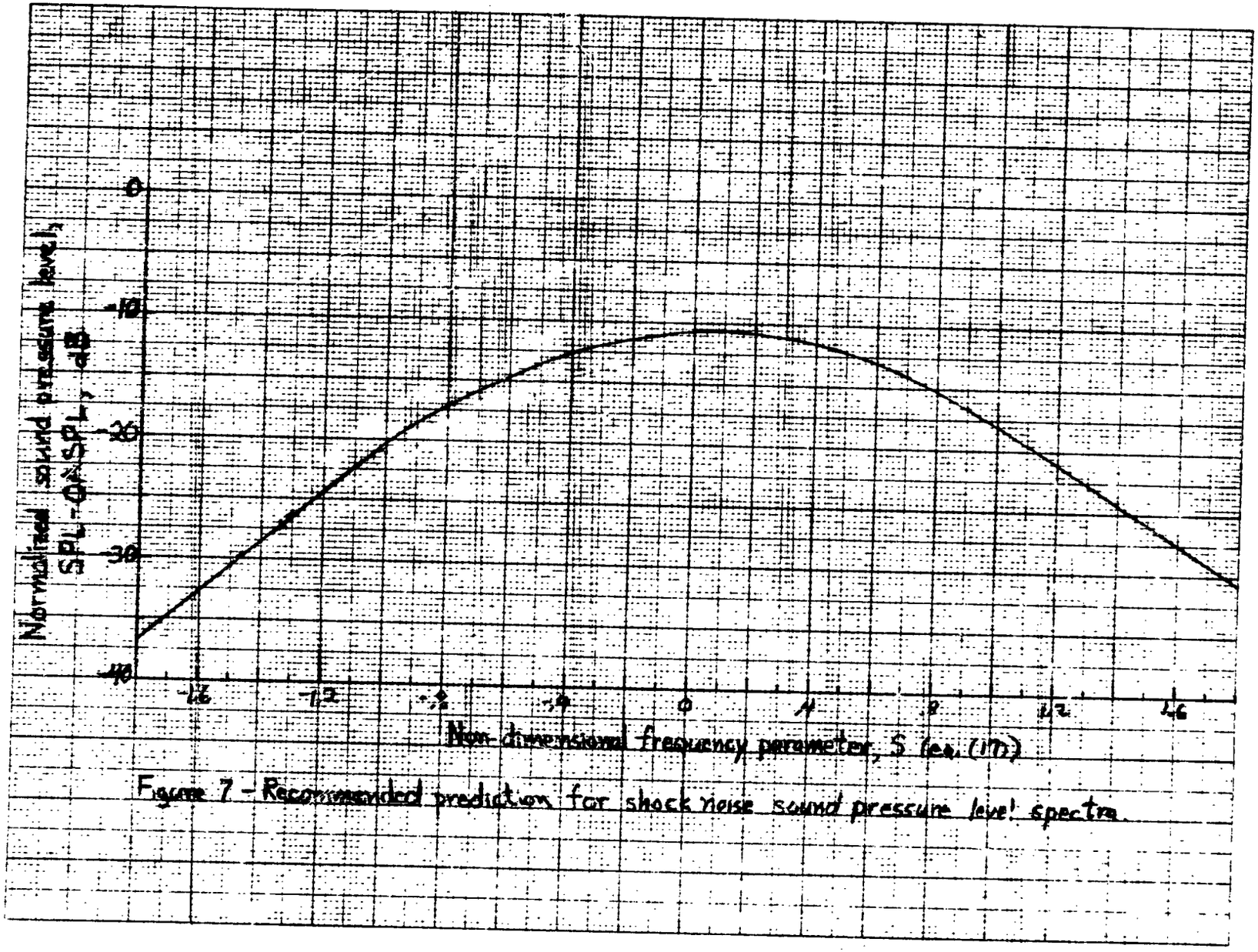

Figure 7 – Recommended prediction for shock noise sound pressure level spectra.

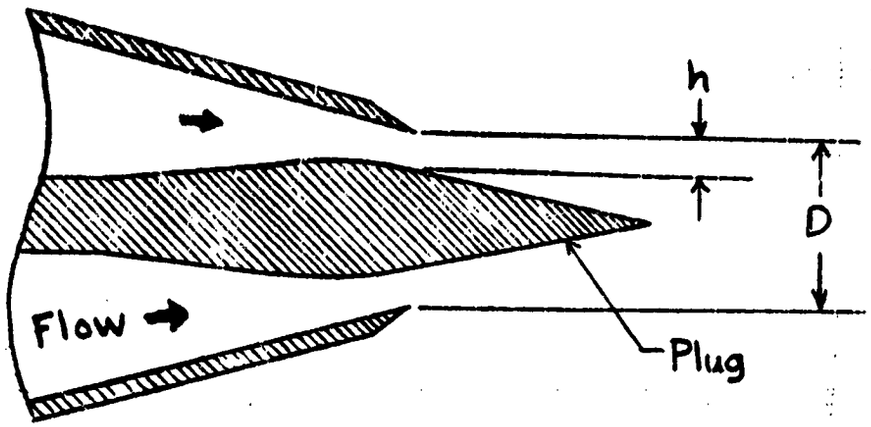

Equivalent diameter, $D_e = 2\sqrt{Dh - h^2}$

Hydraulic diameter, $D_h = 2h$

Diameter ratio, $\frac{D_h}{D_e} = \sqrt{\frac{(h/D)}{1-(h/D)}}$

Figure 8.- Plug nozzle geometric variables.

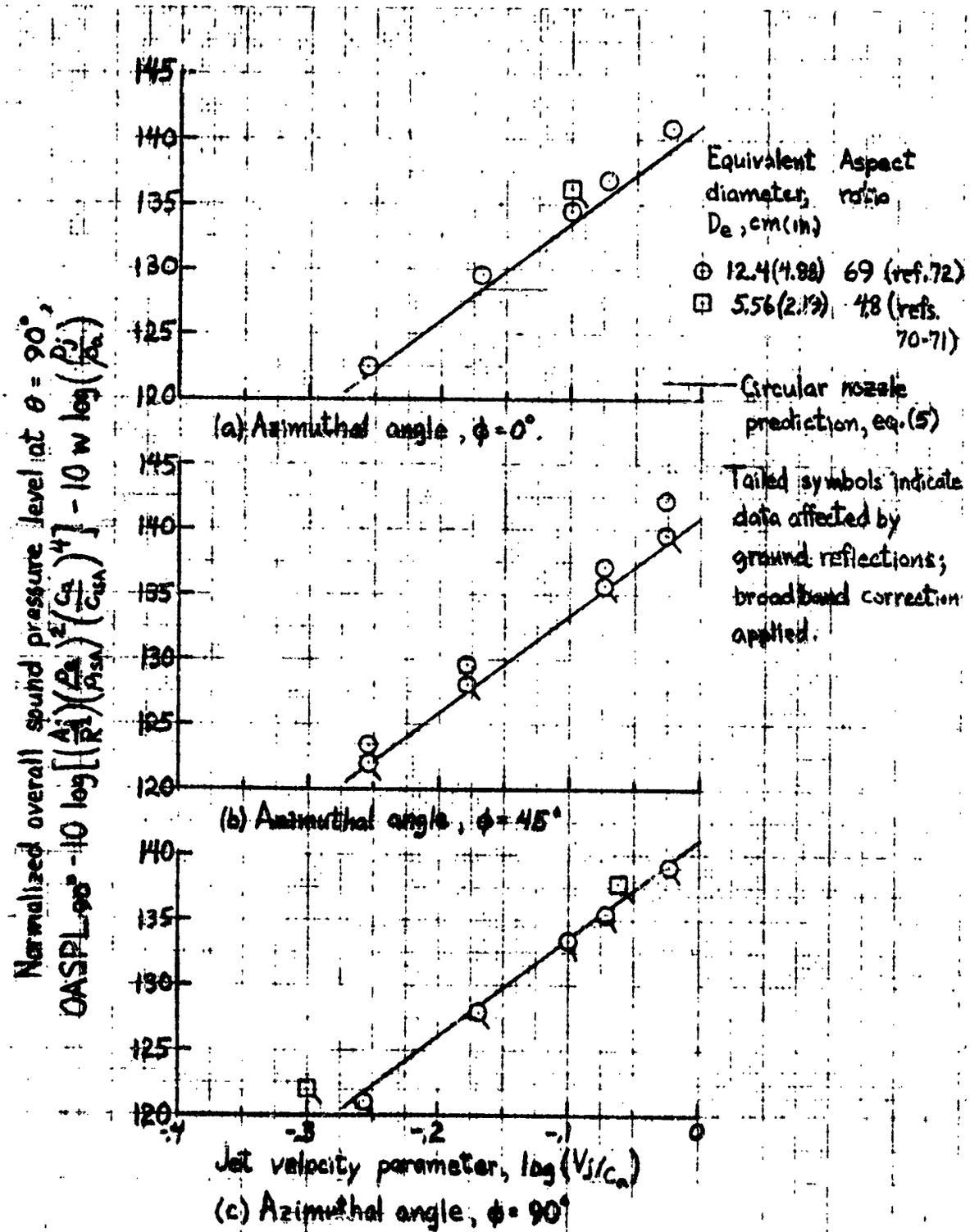

Figure 9.- Prediction of overall sound pressure level at θ = 90° for shock-free slot nozzles and comparison with data for cold-flow tests.

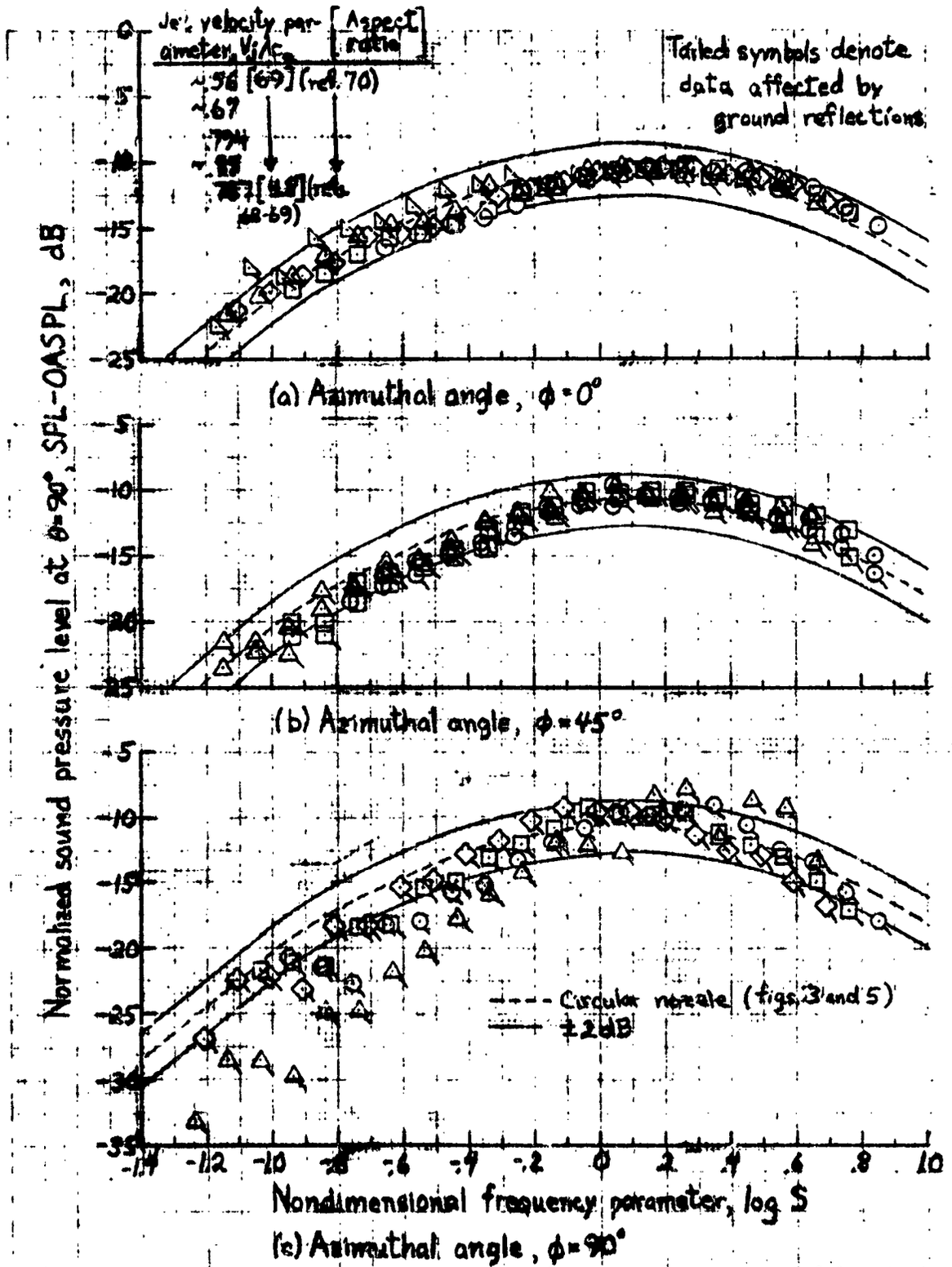

Figure 10.- Prediction of sound pressure level spectra at $\theta = 90°$ for shock-free slot nozzles and comparison with ambient-temperature experimental data.

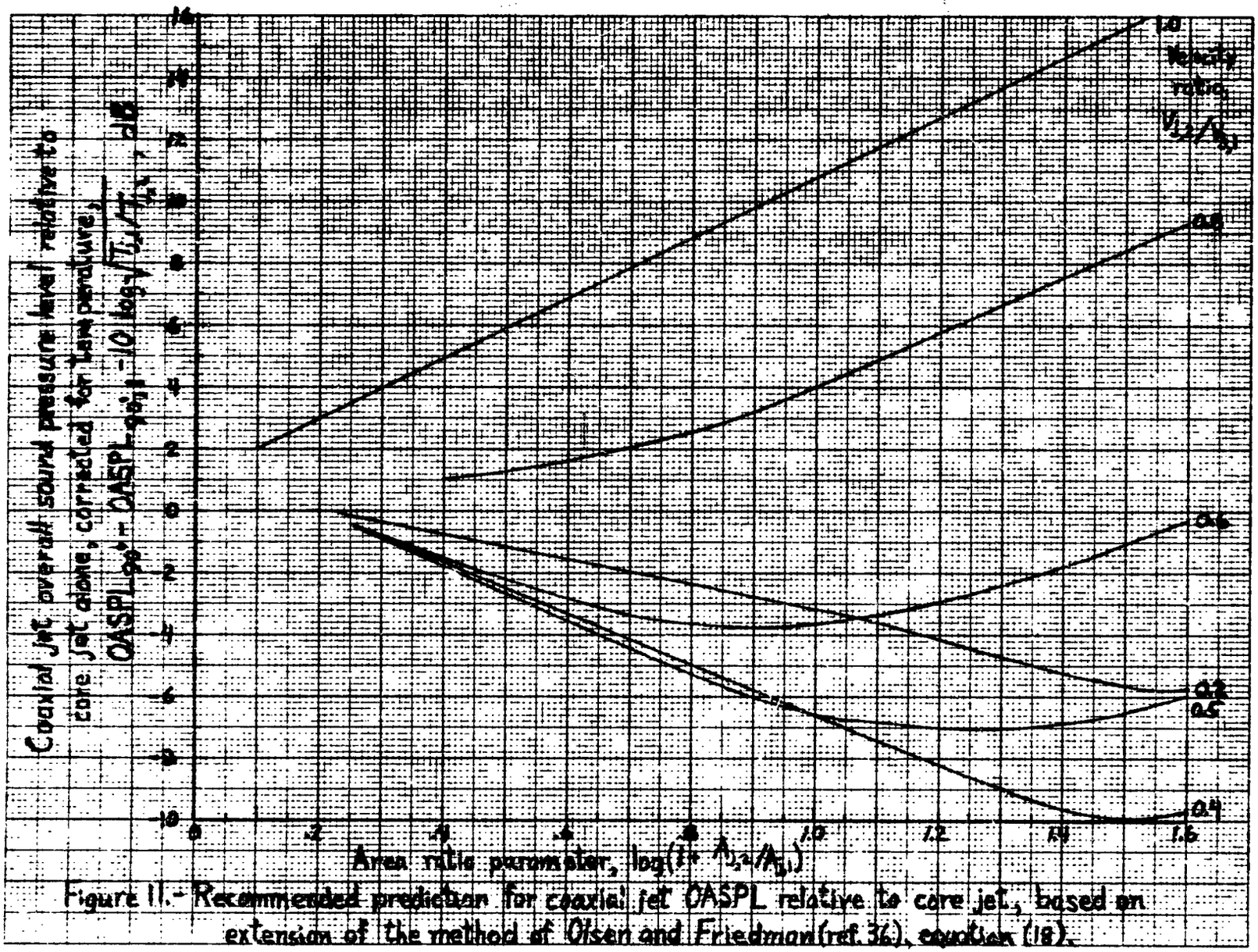

Figure 11.- Recommended prediction for coaxial jet OASPL relative to core jet, based on extension of the method of Olsen and Friedman (ref. 36), equation (18).

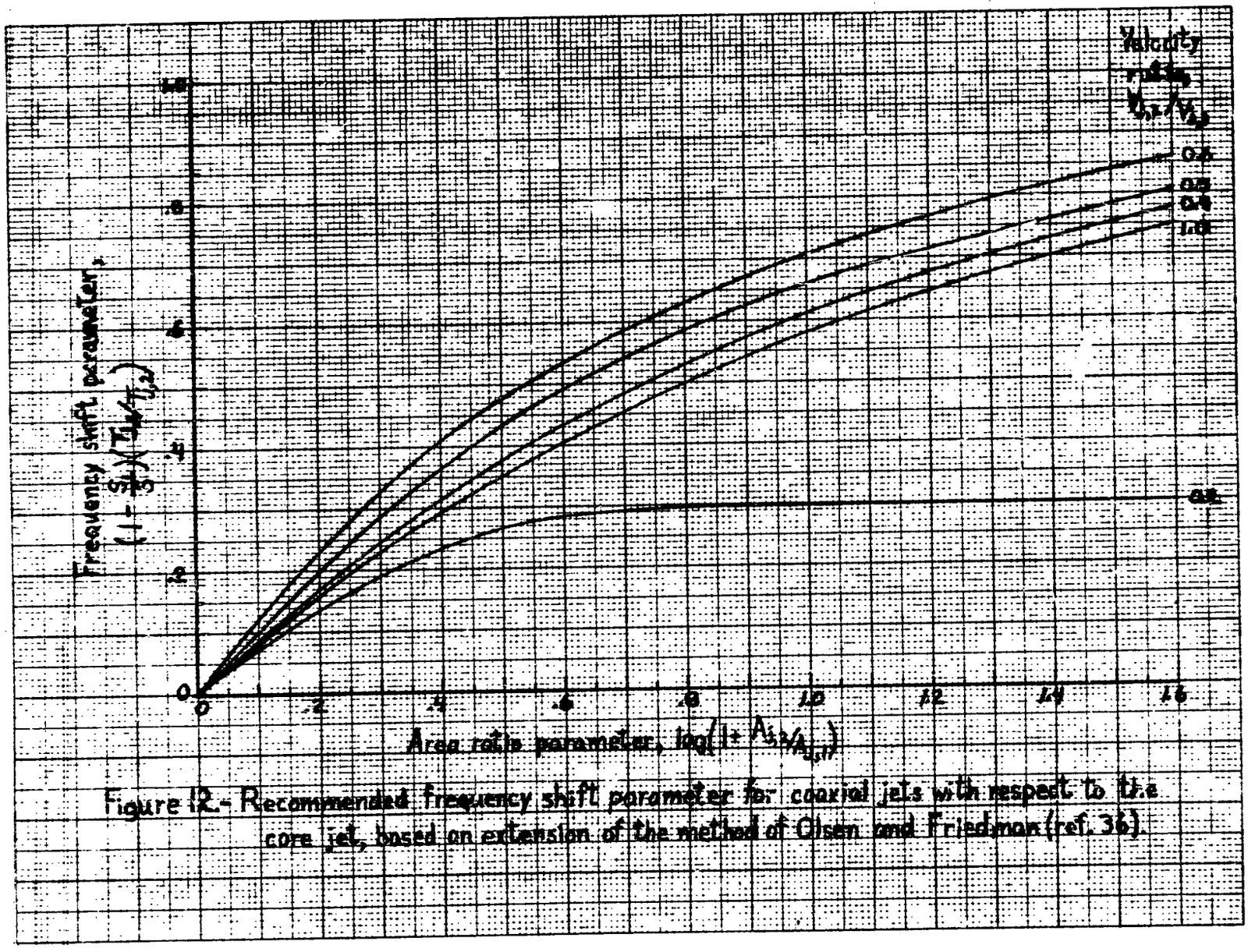

Figure 12.- Recommended frequency shift parameter for coaxial jets with respect to the core jet, based on extension of the method of Olsen and Friedman (ref. 36).

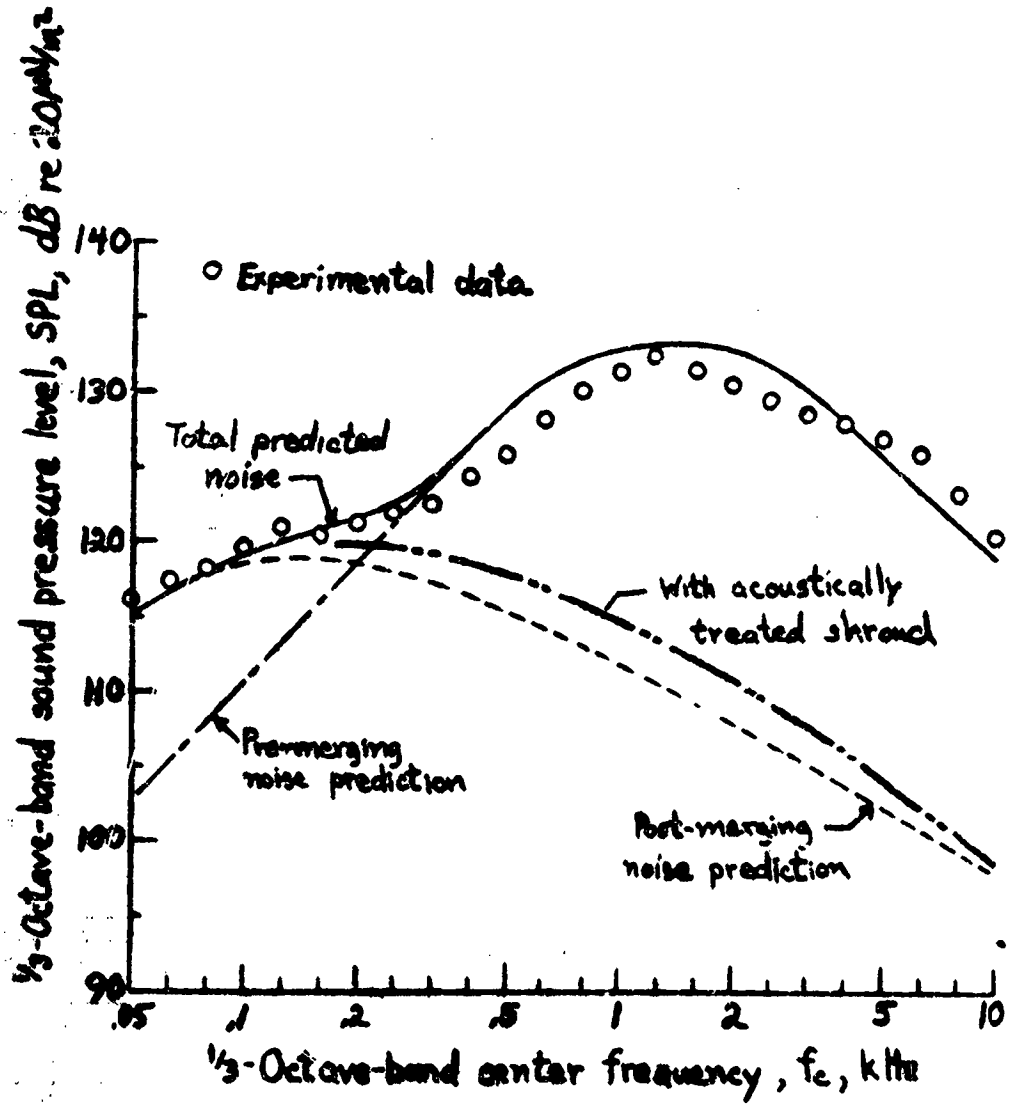

Figure 11.- Multi-tube suppressor nozzle noise spectrum; comparison of experimental data and prediction. 37 tube nozzle on YJ75 engine; nozzle-to-base area ratio 3.3; $\theta = 120°$; no relative velocity; nozzle exit area, $A_j = 0.352\ m^2\ (3.78\ ft^2)$; jet total temperature, $T_j = 703\ K\ (1265°R)$; engine pressure ratio, 2.04 (from ref. 38)

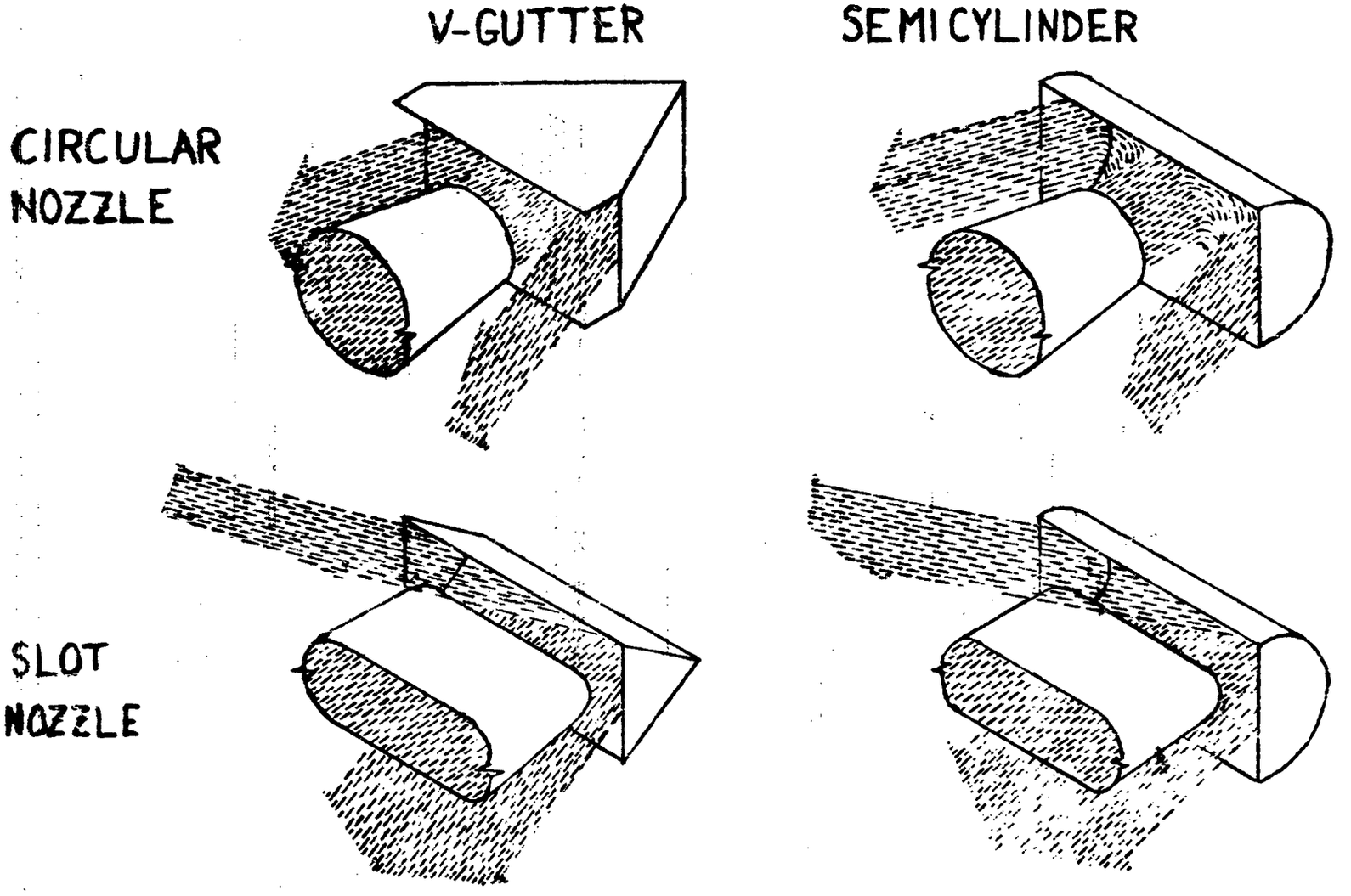

Figure 14.- Small-scale target-type thrust reversers tested with nominal 5-cm (2-in.) nozzles.

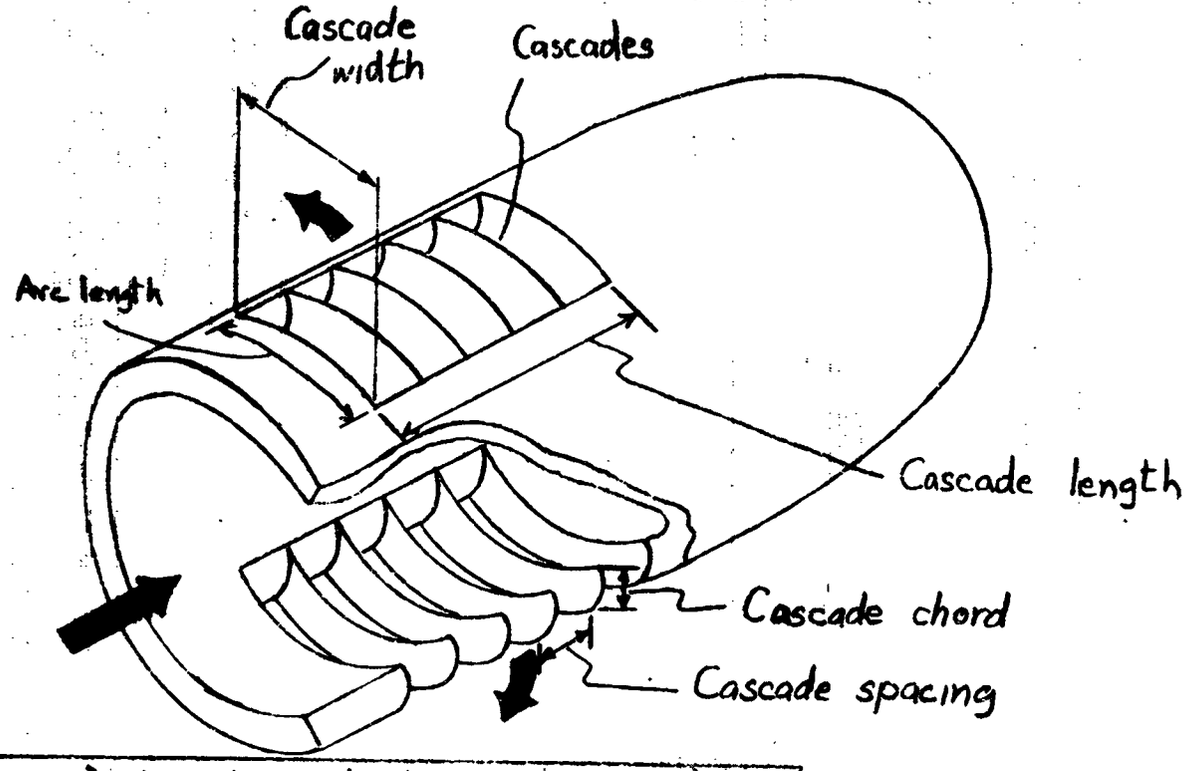

$$D_e = \sqrt{(\text{Number of ports}) \times (\text{Arc length}) \times (\text{Cascade length}) \times \left(\frac{4}{\pi}\right)}$$

$$D_h = 4\,(\text{Arc length}) \times (\text{Cascade spacing}) / [2(\text{Arc length}) + 2\,(\text{Cascade spacing})]$$

Figure 15. - Tail-pipe cascade thrust reverser.

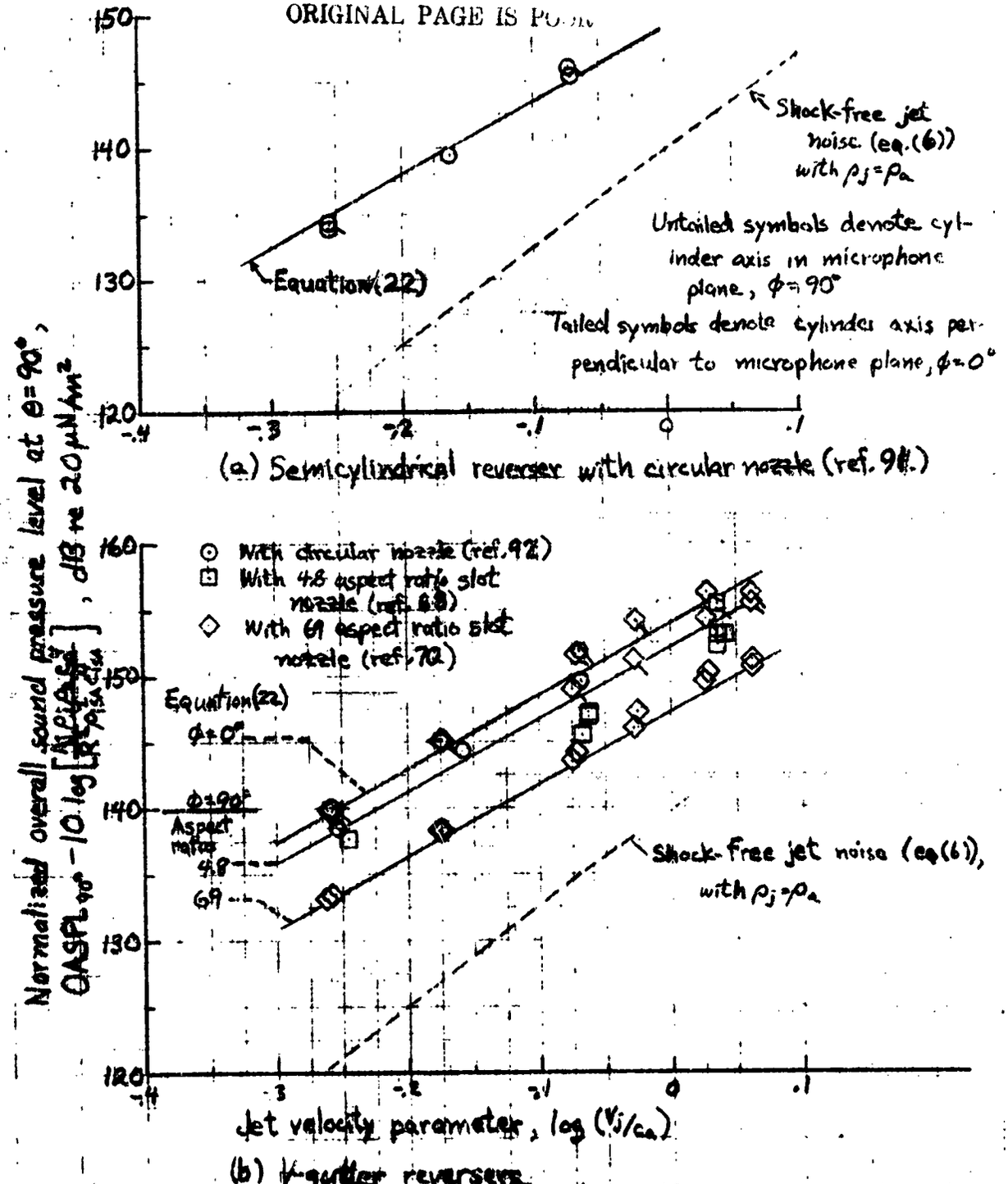

Figure 16.- Prediction of normalized overall sound pressure level at $\theta = 90°$ for target-type thrust reversers and comparison with experimental data.

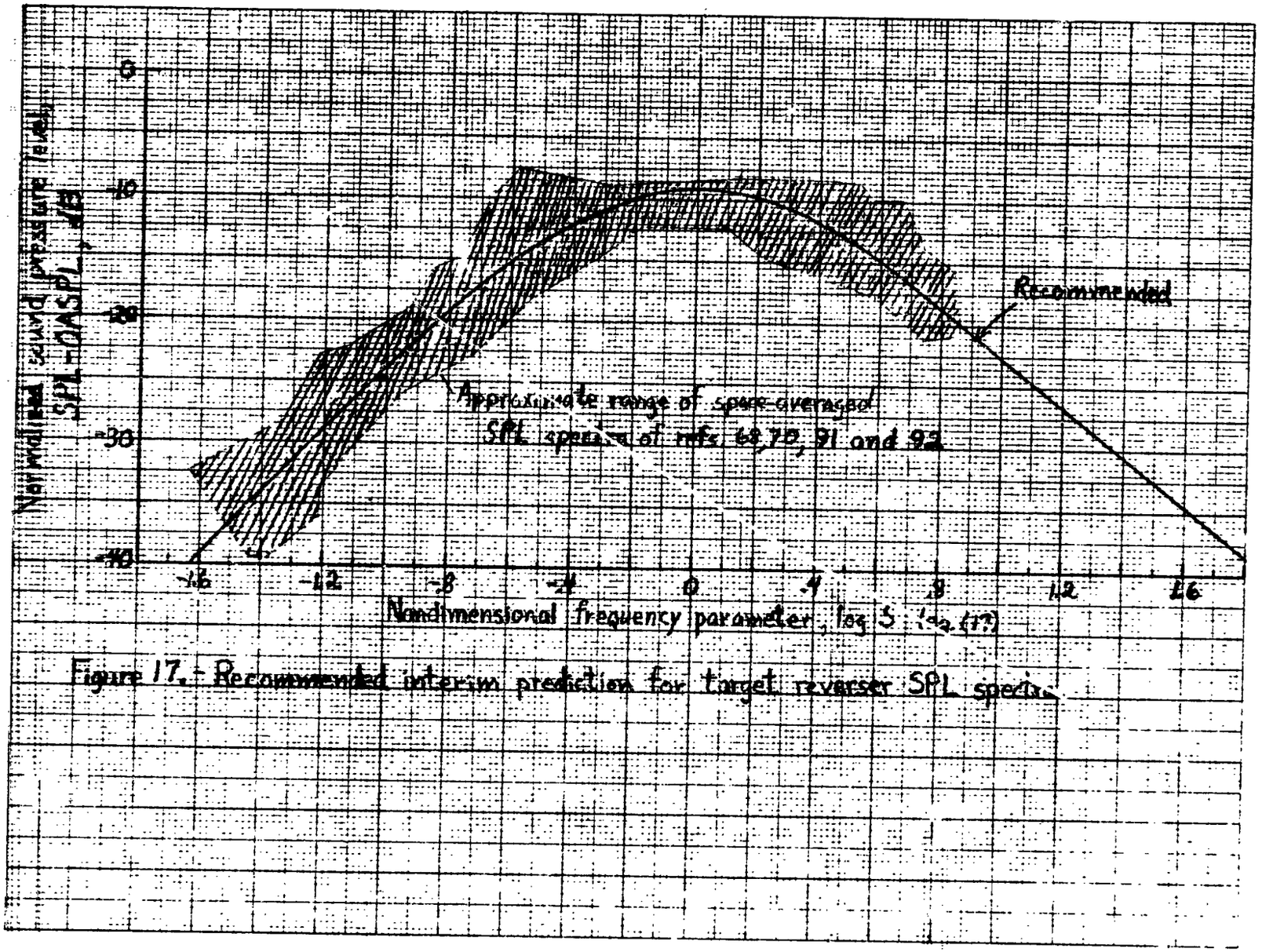

Figure 17.- Recommended interim prediction for target reverser SPL spectra.

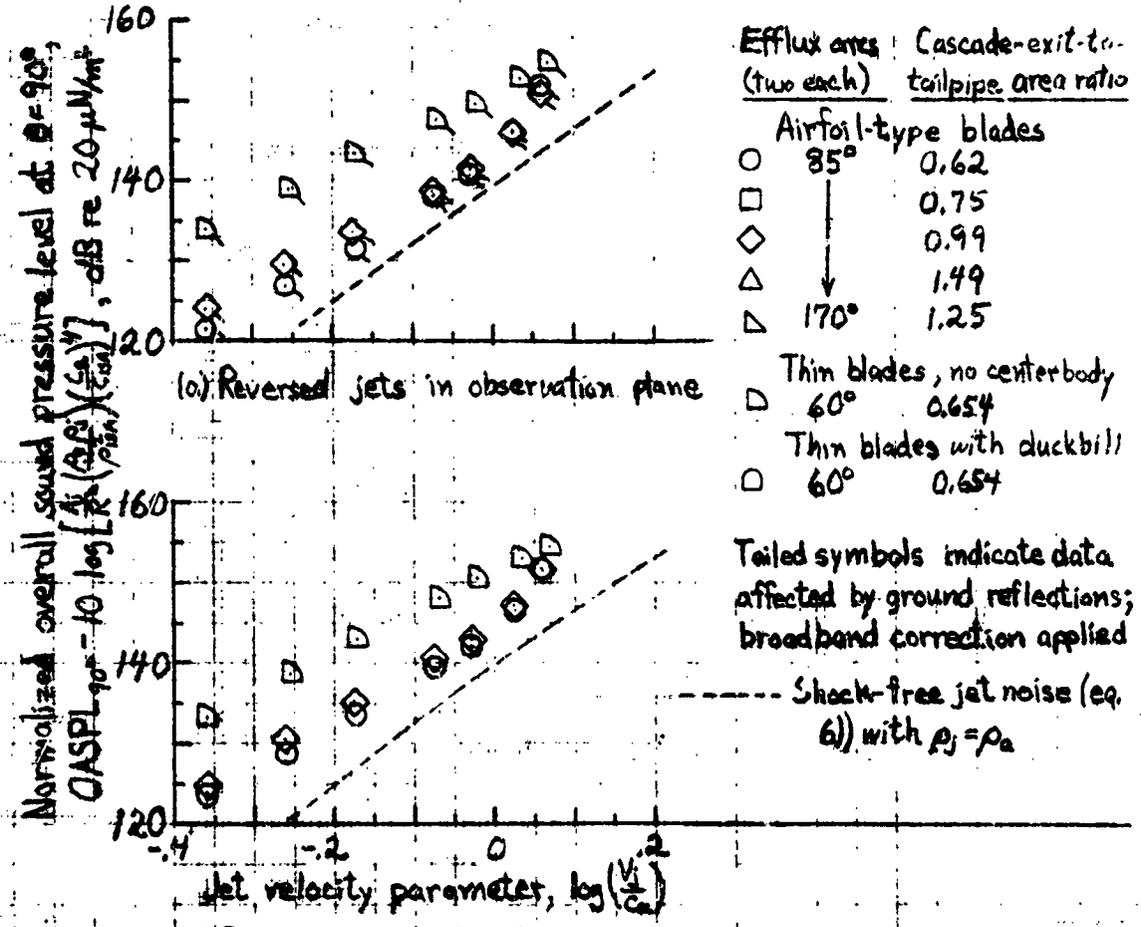

Figure 18.- Overall sound pressure level at $\theta = 90°$ for cascade reversers.

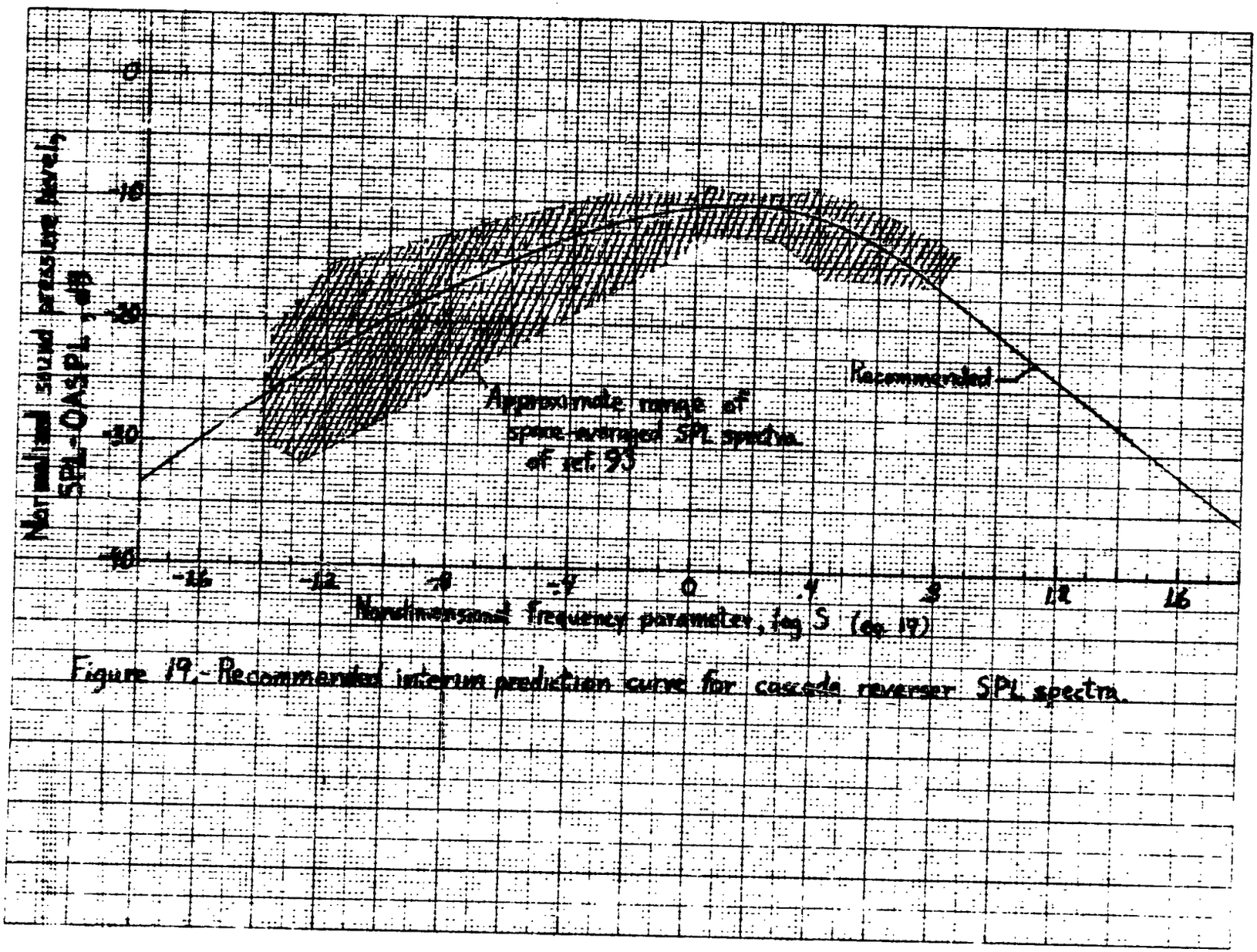

Figure 19.- Recommended interim prediction curve for cascade reverser SPL spectra.

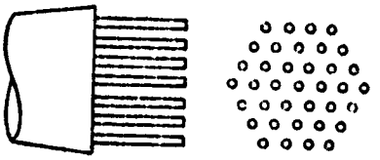

Multi-tube suppressor nozzle

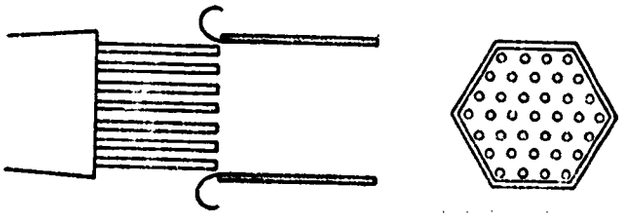

Multi-tube nozzle with ejector

Figure 20.- Typical ejector/suppressor system.

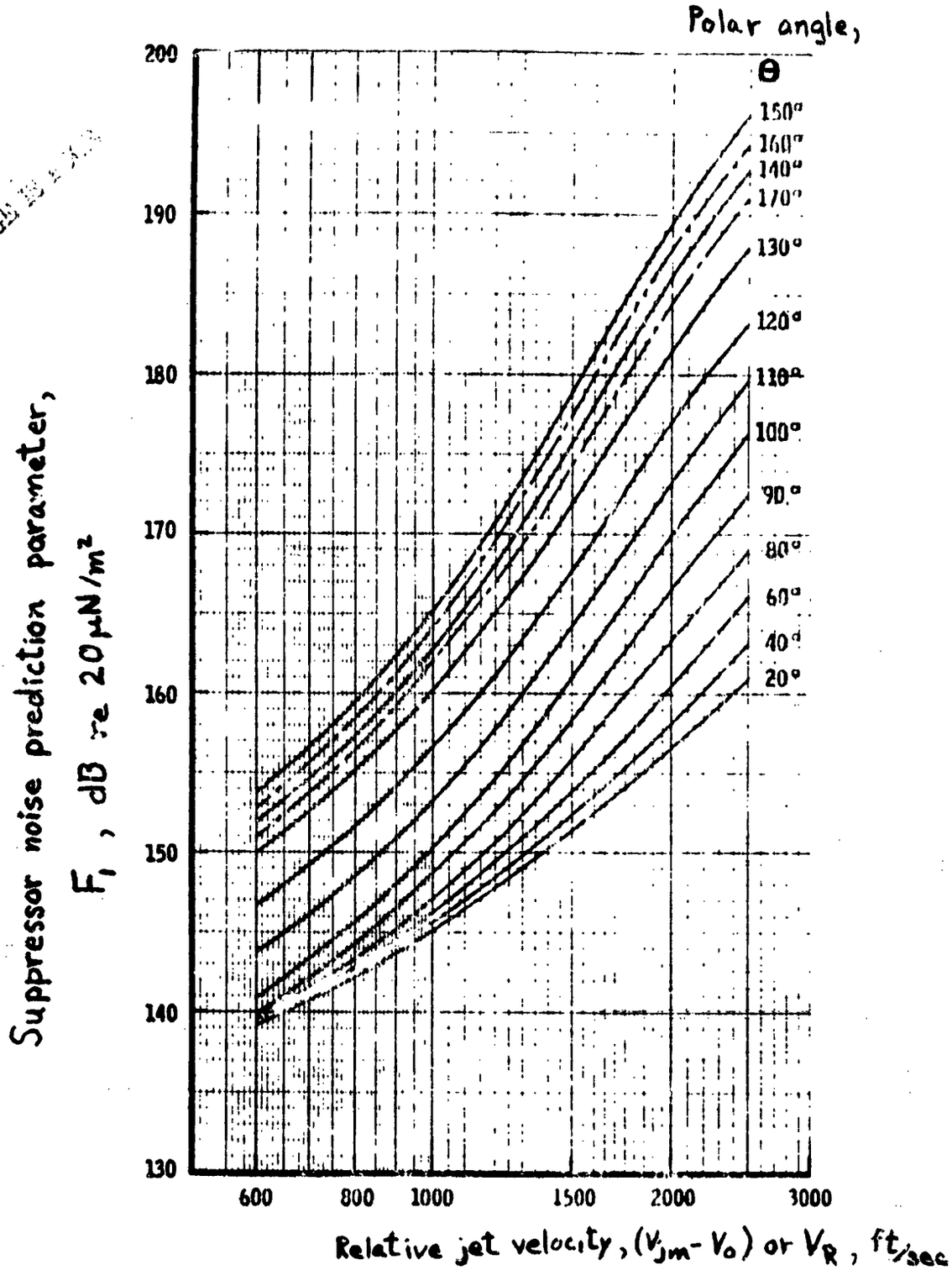

Figure 21.- Suppressor noise prediction parameter as function of relative jet velocity for post-merging jet noise prediction. Data from full-scale JT8D engine and hot 45.6-cm² (0.0491-ft²) exit-area model (ref. 38).

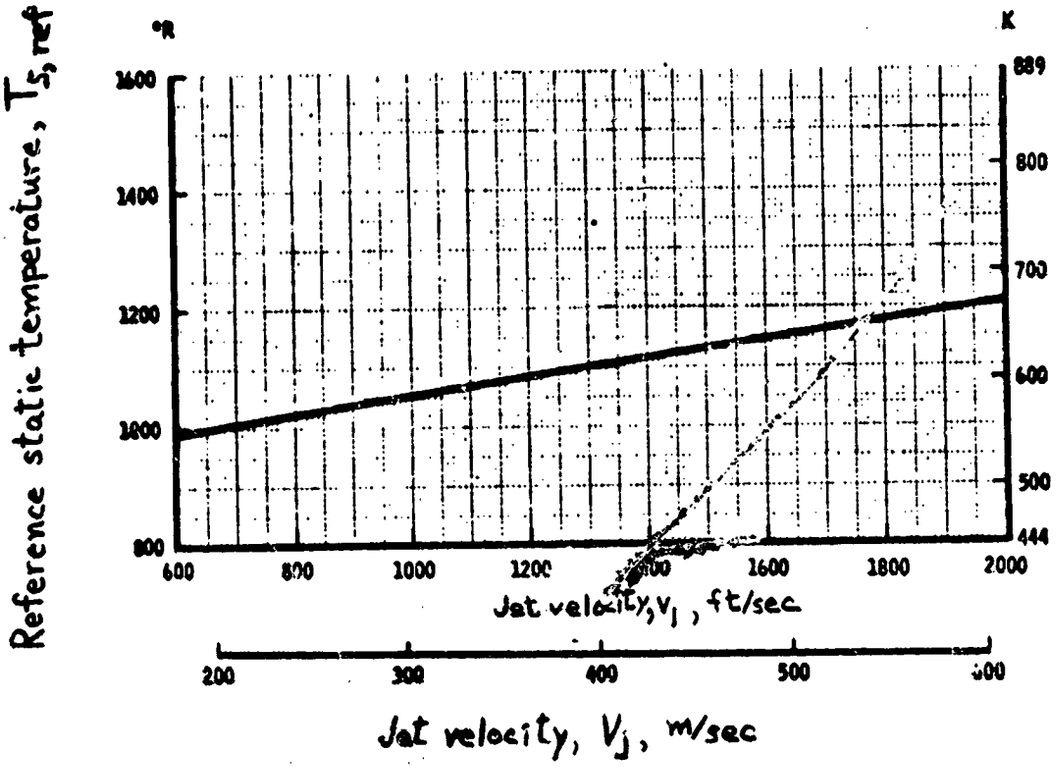

Figure 22.- Reference static temperature as function of jet velocity (ref. 38).

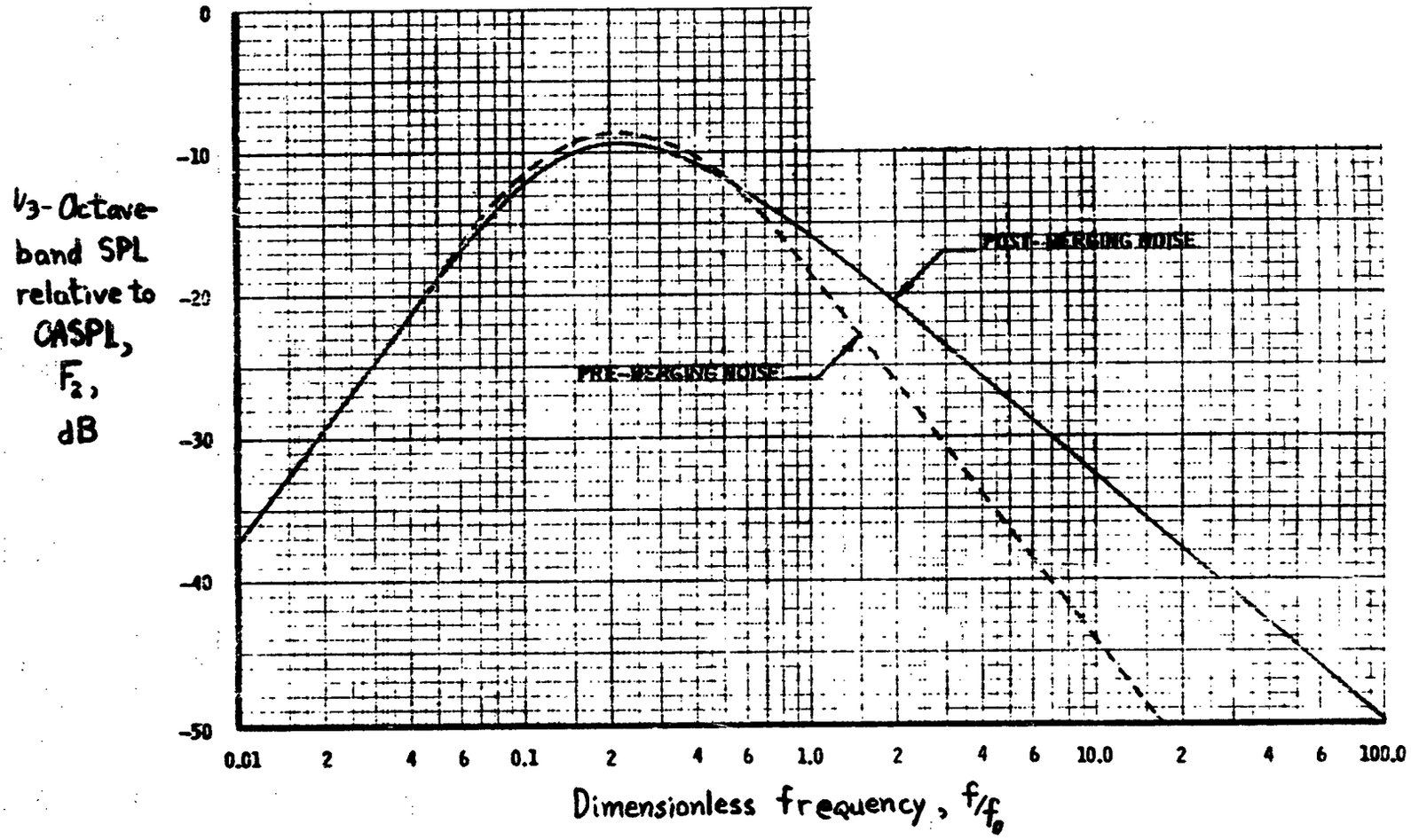

Figure 23. - Index spectrum shape (ref. 38).

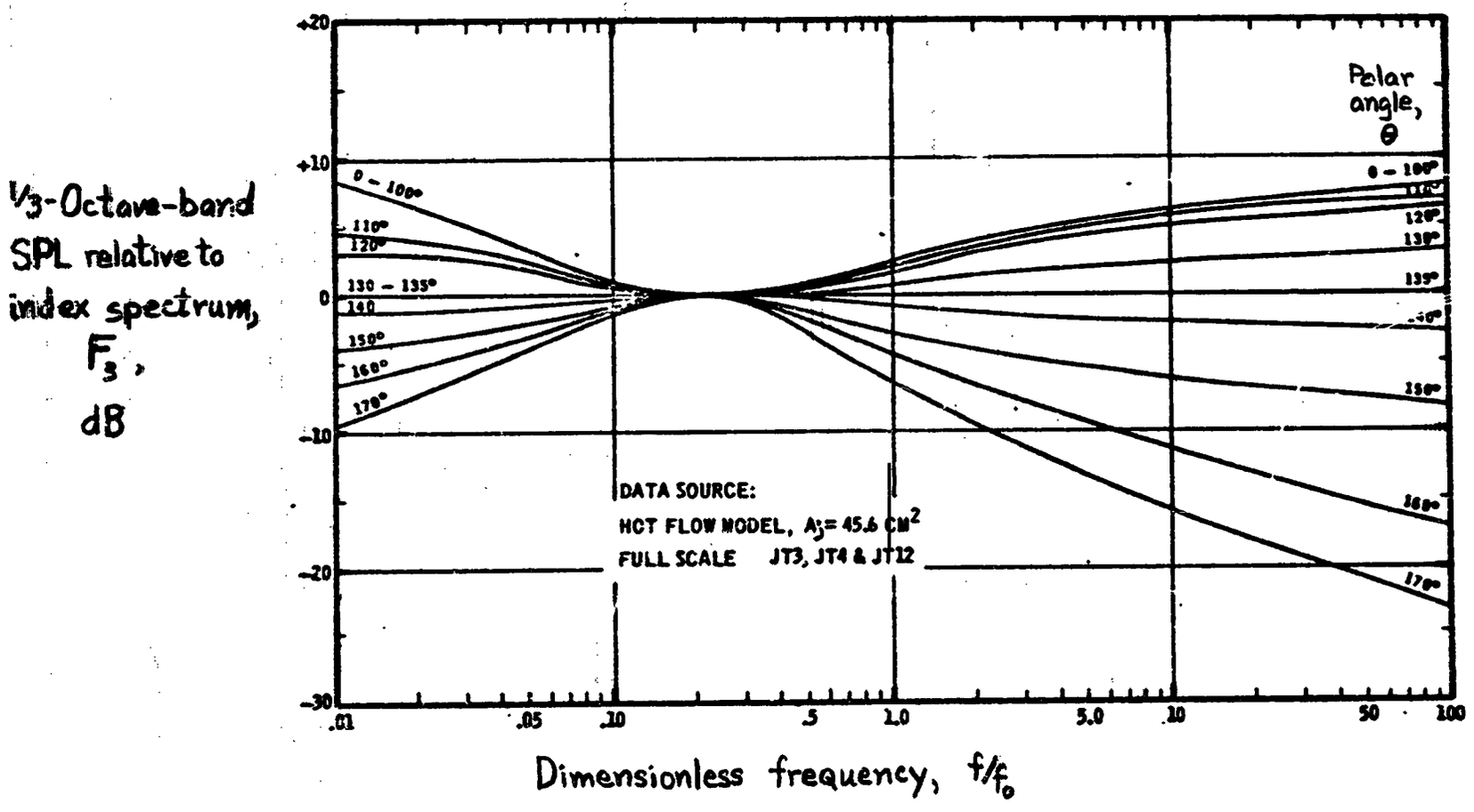

Figure 24. - Spectrum directivity corrections (ref. 38).

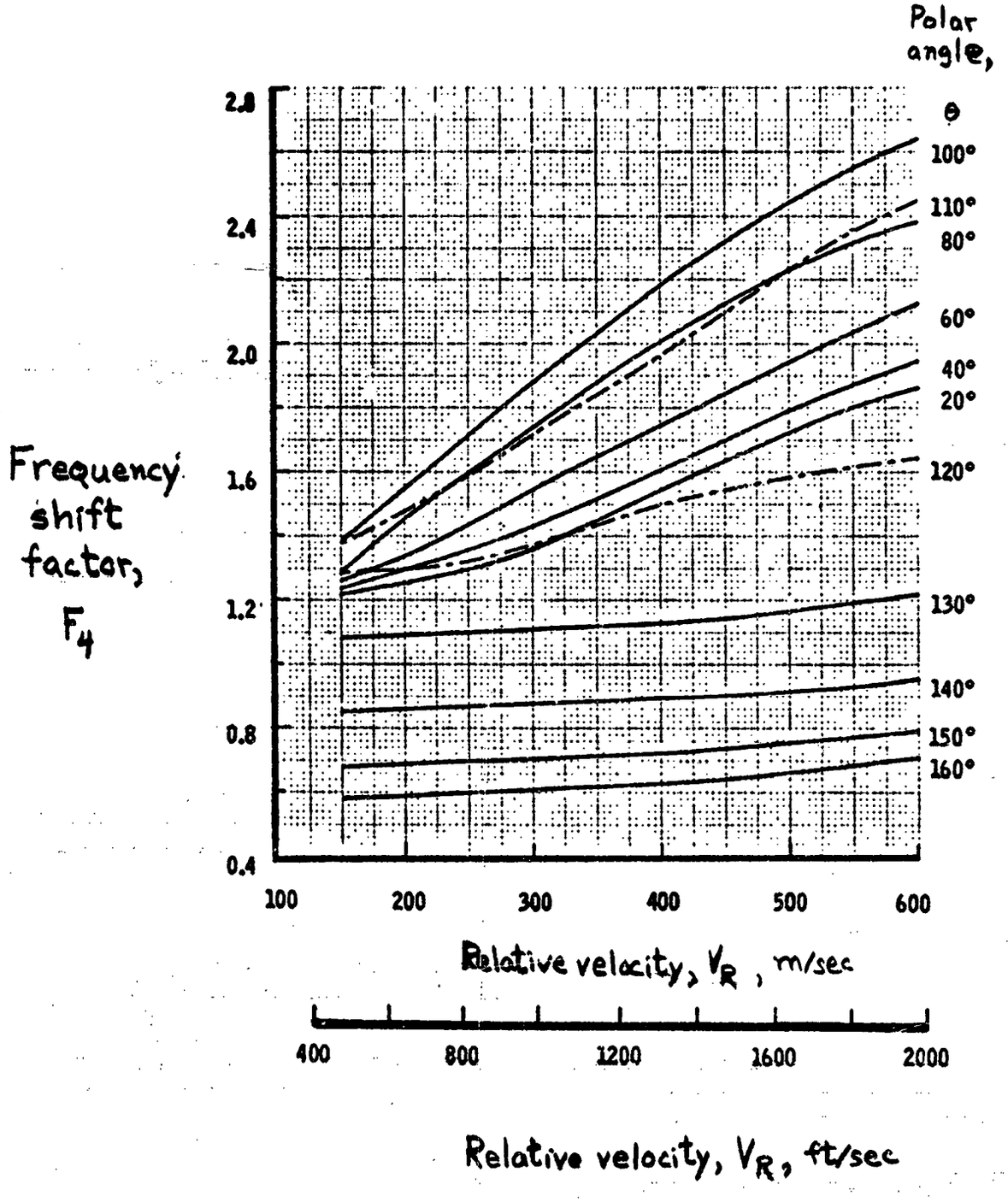

Figure 25. - Frequency shift due to convection (ref. 38).

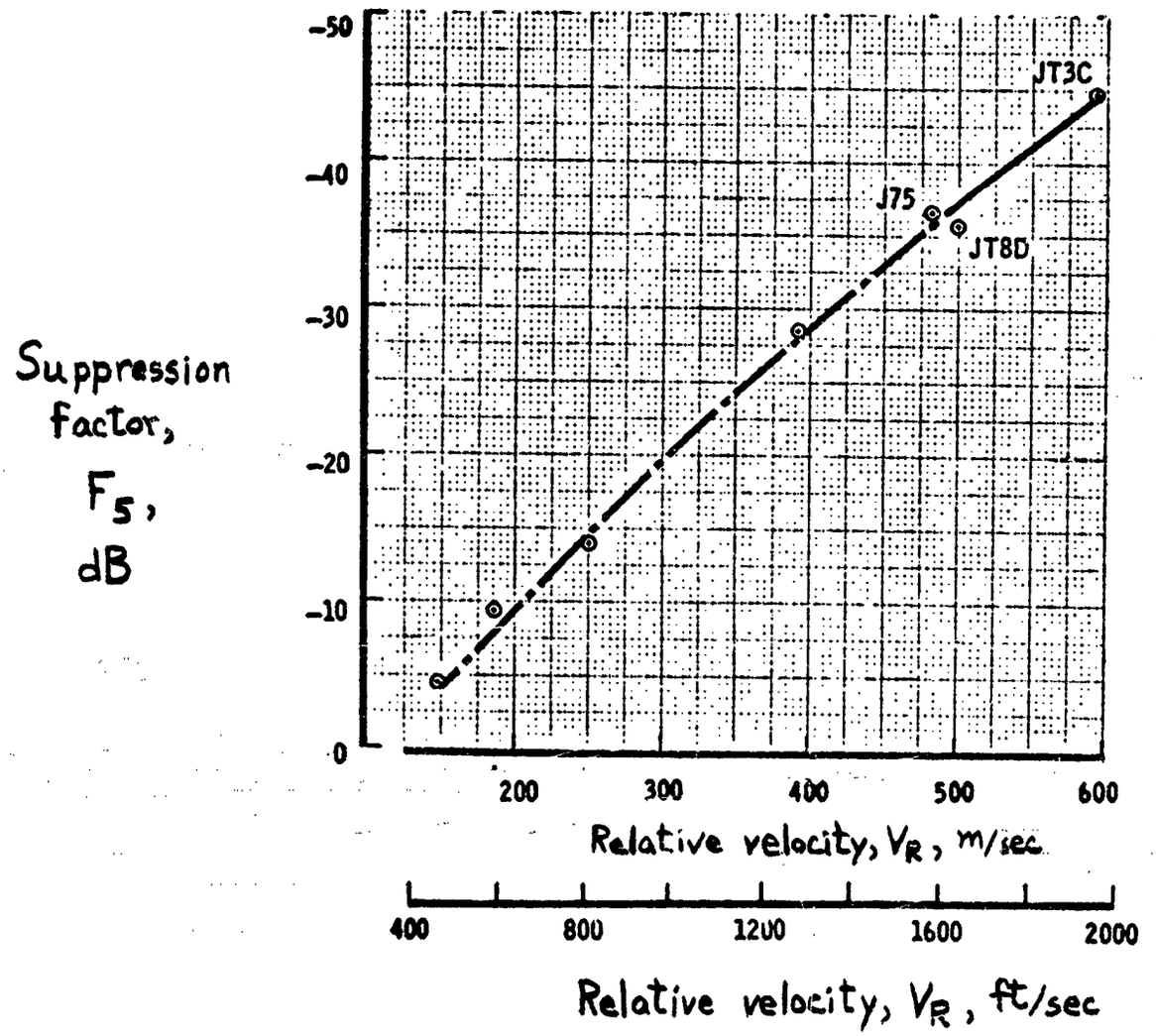

Figure 26.- Post-merging suppression factor as function of relative velocity for bare suppressor configuration (ref. 38).

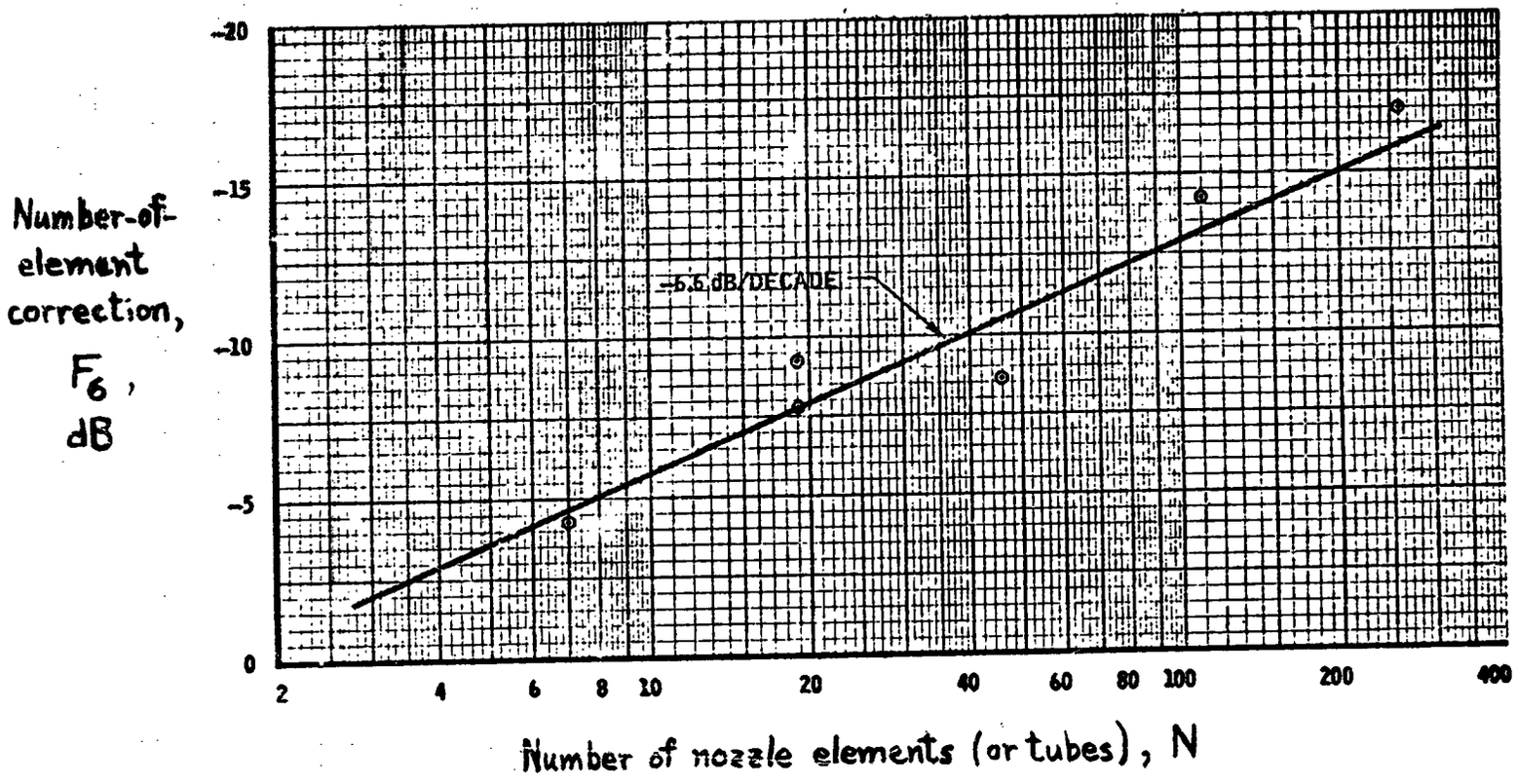

Figure 27.- Effect of number of elements on suppression (ref. 38).

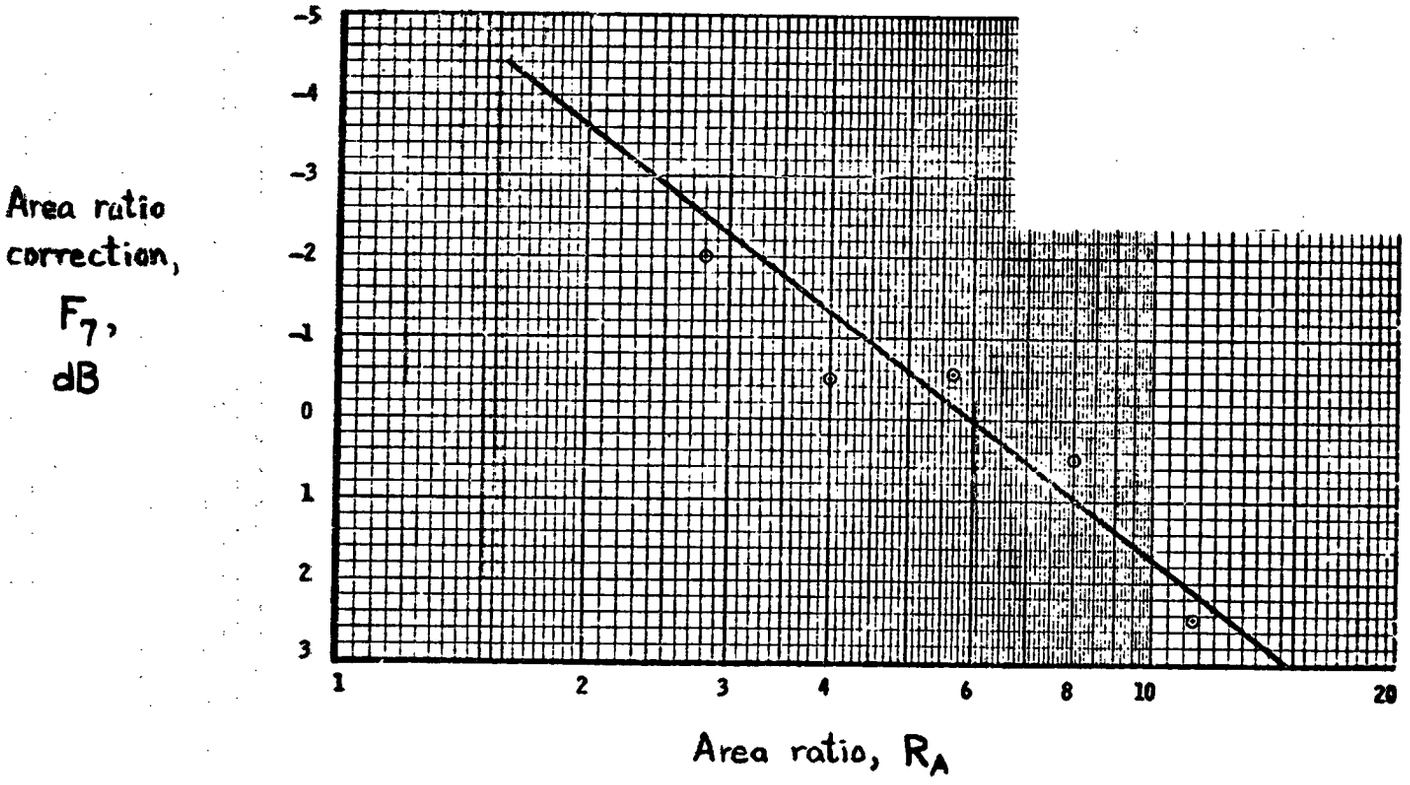

Figure 28.- Effect of area ratio on suppression (ref. 38).

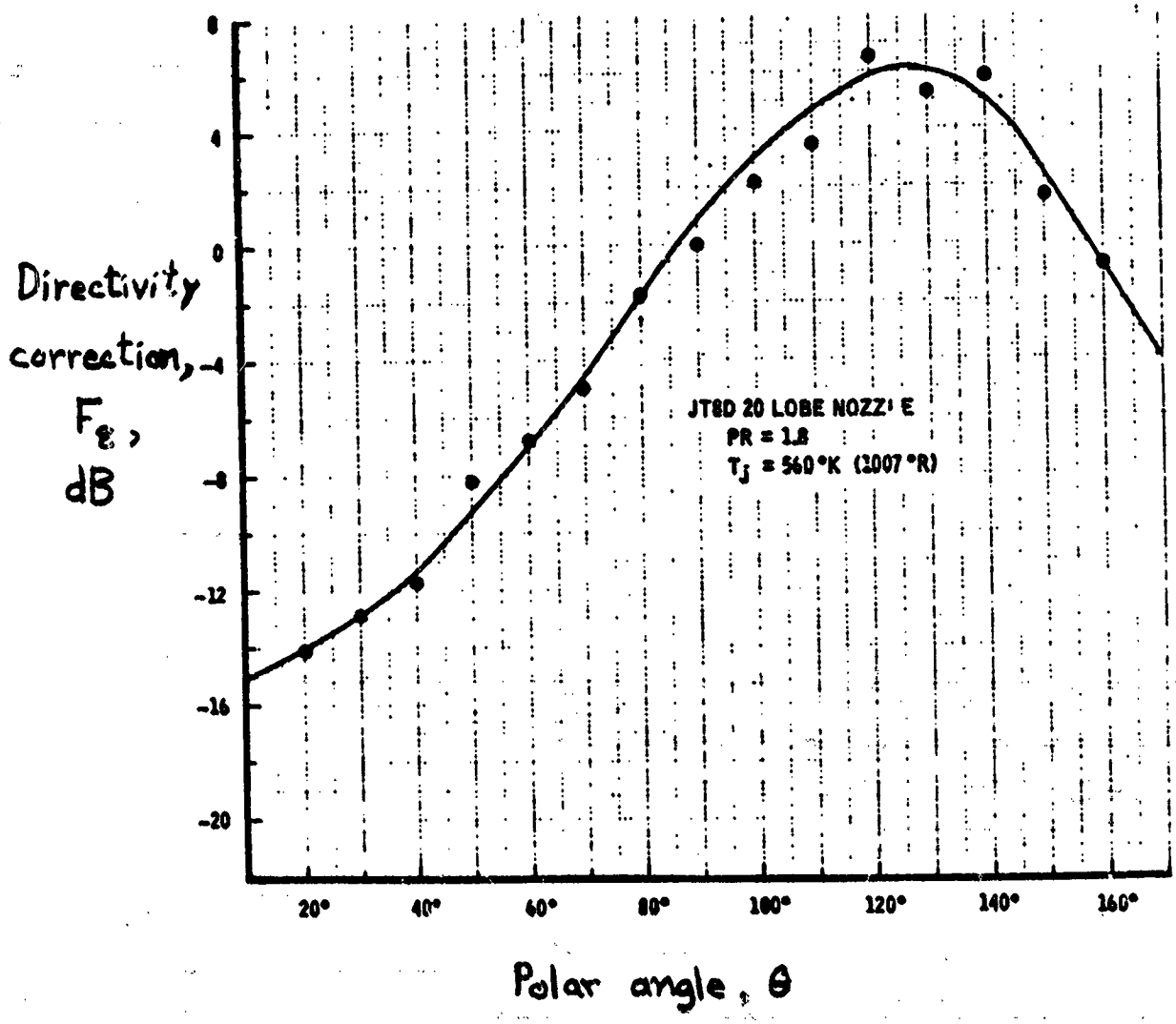

Figure 29 - Pre-merging noise directivity correction (ref. 38).

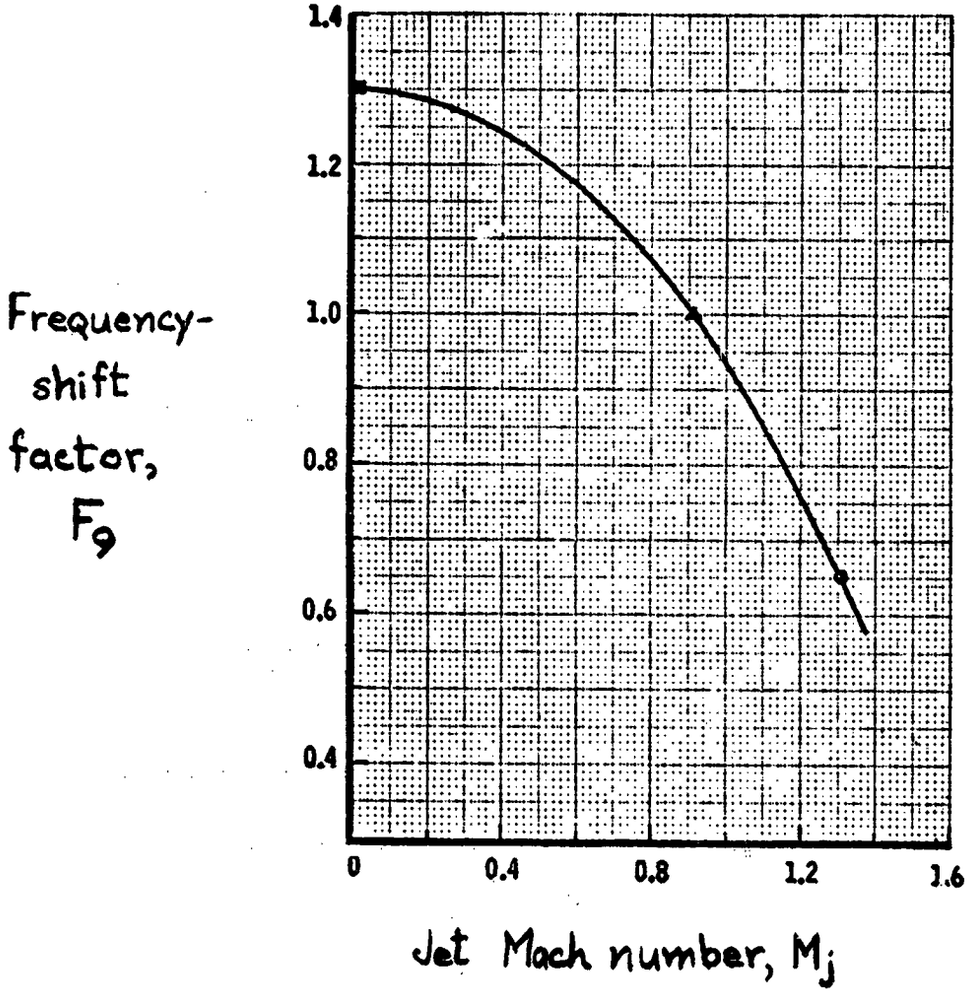

Figure 30.- Frequency shift due to refraction and core change(ref. 38)

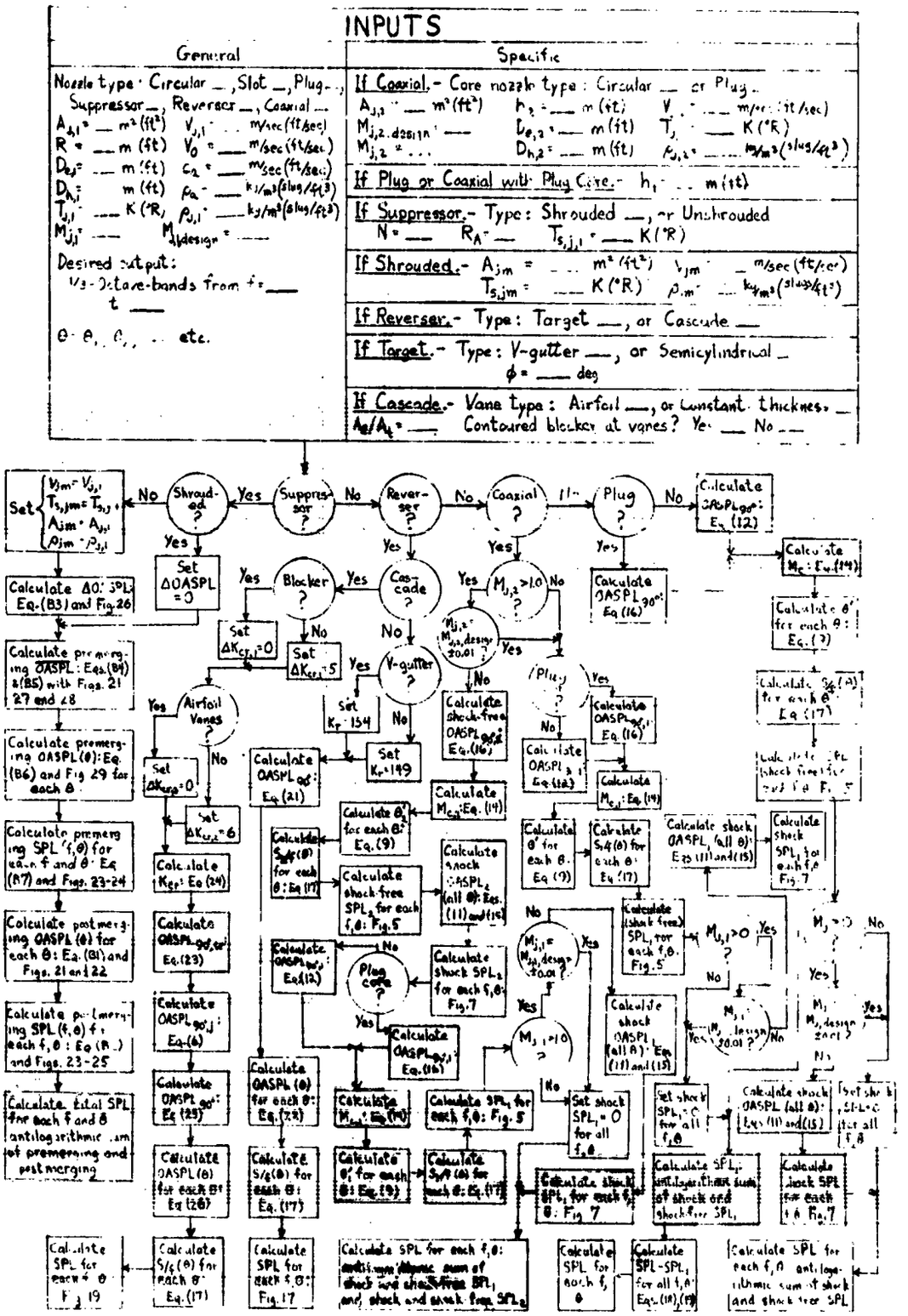

Figure 31.- Calculation flow chart.